

EVOLUTION OF MOLECULAR ABUNDANCES IN PROTO-PLANETARY DISKS WITH ACCRETION FLOW

YURI AIKAWA

Department of Physics, The Ohio State University, Columbus, OH 43210

TOYOHARU UMEBAYASHI

Computing Service Center, Yamagata University, Yamagata 990-8560, Japan

TAKENORI NAKANO¹

Nobeyama Radio Observatory, National Astronomical Observatory, Nobeyama, Minamisaku, Nagano 384-1305, Japan

AND

SHOKEN M. MIYAMA

National Astronomical Observatory, Mitaka, Tokyo 181-8588, Japan

Received 1998 October 9; accepted 1999 February 17

ABSTRACT

We investigate the evolution of molecular abundances in a protoplanetary disk in which matter is accreting toward the central star by solving numerically the reaction equations of molecules as an initial-value problem. We obtain the abundances of molecules, both in the gas phase and in ice mantles of grains, as functions of time and position in the disk. In the region of surface density less than 10^2 g cm^{-2} (distance from the star $\gtrsim 10 \text{ AU}$ for the mass accretion rate $10^{-8} M_{\odot} \text{ yr}^{-1}$), cosmic rays are barely attenuated even on the midplane of the disk and produce chemically active ions such as H_3^+ and He^+ . We find that through reactions with these ions considerable amounts of CO and N_2 , which are initially the dominant species in the disk, are transformed into CO_2 , CH_4 , NH_3 , and HCN. In the regions where the temperature is low enough for these products to freeze onto grains, they accumulate in ice mantles. As the matter migrates toward inner warmer regions of the disk, some of the molecules in the ice mantles evaporate. It is found that most of the molecules desorbed in this way are transformed into less volatile molecules by the gas-phase reactions, which then freeze out. Molecular abundances both in the gas phase and in ice mantles crucially depend on the temperature and thus vary significantly with the distance from the central star. Although molecular evolution proceeds in protoplanetary disks, our model also shows that significant amount of interstellar ice, especially water ice, survives and is included in ice mantles in the outer region of the disks. We also find that the timescale of molecular evolution is dependent on the ionization rate and the grain size in the disk. If the ionization rate and the grain size are the same as those in molecular clouds, the timescale of the molecular evolution, in which CO and N_2 are transformed into other molecules, is about 10^6 yr , which is slightly smaller than the lifetime of the disk. The timescale for molecular evolution is larger (smaller) in the case of lower (higher) ionization rate or larger (smaller) grain size. We compare our results with the molecular composition of comets, which are considered to be the most primitive bodies in our solar system. The molecular abundances derived from our model naturally explain the coexistence of oxidized ice and reduced ice in the observed comets. Our model also suggests that comets formed in different regions of the disk have different molecular compositions. Finally, we give some predictions for future millimeter-wave and sub-millimeter-wave observations of protoplanetary disks.

Subject headings: circumstellar matter — ISM: abundances — ISM: molecules —
solar system: formation — stars: formation — stars: pre-main-sequence

1. INTRODUCTION

The theoretical study of the evolution of molecular abundances in protoplanetary disks is important from various points of view. First, it will directly show the composition of material the bodies in planetary systems are made from. The molecular composition determines some of the basic properties of planets such as density, thermal history, and atmospheric composition. Knowledge of the molecular composition at each radius of the disk is helpful in understanding and predicting the properties of individual planets formed therein.

Second, the theoretical study of molecular evolution is of great help to obtaining the physical states of the protoplanetary disks from molecular line observations. Recent radio

observations have produced great progress in the study of protoplanetary disks. For example, emission lines of molecules such as CO, CN, and HCO^+ have recently been detected for some T Tauri stars (Skrutskie et al. 1993; Guilloteau & Dutrey 1994; Handa et al. 1995; Dutrey, Guilloteau, & Guélin 1997), and the aperture-synthesis imagings have directly revealed the distribution of CO around some T Tauri stars in the Taurus molecular cloud with a spatial resolution of a few hundred AU (Kawabe et al. 1993; Koerner, Sargent, & Beckwith 1993; Dutrey, Guilloteau, & Simon 1994; Koerner & Sargent 1995; Saito et al. 1995). Moreover, the future sub-millimeter arrays will enable us to observe the disks with higher spatial resolution and thus to observe more precisely the structure and evolution of protoplanetary disks.

Combining observational data with theoretical studies of molecular abundances will help determine the initial condi-

¹ Present address: Department of Physics, Kyoto University, Kyoto 606-8502, Japan.

tions and the process of planet formation. In particular, we will be able to find out when and how the gaseous component in the disk disappears by comparing disks in various evolutionary stages. The gaseous component in our primitive solar nebula must have disappeared at some stage of planet formation. The mechanism of this gaseous dissipation is not yet well understood, though some mechanisms have been suggested such as photoevaporation by irradiation from the central star (Shu, Johnstone, & Hollenbach 1993) and the tidal effect of protoplanets (Takeuchi, Miyama, & Lin 1996). Observations of the gaseous component in various disks can provide critical constraints on the mechanism of dissipation and thus on the mechanism and timescale of planet formation. However, derivation of some physical quantities from molecular line observations requires the help of theoretical study on molecular evolution. For instance, the amount of the gaseous component in the disk is estimated by observations of molecules other than the main component H_2 , because H_2 does not emit photons except at the very inner region of the disk (radius $R \lesssim 0.1$ AU).

Third, molecular abundances can be a useful probe in investigating the formation processes of our own solar system. Ultimately, we can constrain the processes, places, and epochs of the formation of primitive bodies, such as comets, by comparing their molecular composition with the theoretical results on the distribution and evolution of molecular abundances in the disk. Comets are the most primitive among the existing bodies in our solar system and are now considered to be remnants of icy planetesimals formed in the outer region of the solar system ($R \gtrsim 20$ AU). Various molecular species, such as CO, NH_3 , and HCN, have recently been detected in comet Hyakutake and comet Hale-Bopp (Crovisier 1998 and references therein). In addition, from a statistical study on the molecular composition of comets A'Hearn et al. (1995) found significant compositional groupings of comets, which are apparently related to their formation site. The physical conditions of our solar system in the early stages must have been encoded in cometary compositions.

Some theoretical work has been done on molecular abundances in protoplanetary disks. In their early work Lewis and his colleagues investigated the composition in the disk assuming thermochemical equilibrium (Lewis 1974; Lewis, Barshay, & Noyes 1979). For gas with the solar abundance and for the pressure appropriate to the solar nebula, they predicted that most of the carbon is in the form of CO at $T \gtrsim 700$ K and in the form of CH_4 at lower temperatures and that most of the nitrogen is in the form of N_2 at $T \gtrsim 300$ K and in the form of NH_3 at lower temperatures. This means that the disk should be CO- and N_2 -rich at $R \lesssim 1$ AU and CH_4 - and NH_3 -rich at $R \gtrsim 1$ AU.

It was pointed out, however, that in the region of low temperatures the reaction rates are so low that thermochemical equilibrium cannot be achieved within the timescale of the disk (Lewis & Prinn 1980). Instead of the chemical equilibrium model, Prinn (1993) (and references therein) proposed the "kinetic inhibition model" (hereafter KI model), assuming that the matter at different radius is well mixed by turbulence. Their basic idea is that the molecular abundances in the matter flowing *outward* are "quenched" when the temperature has decreased to a value below which the timescale for chemical reaction is larger than the dynamical timescale. Adopting a dynamical timescale for

the disk of $\sim 10^{13}$ s, they concluded that the molecular abundances are quenched at 850–1500 K ($R < 1$ AU) and that CO and N_2 were the dominant components in the solar nebula.

In this paper we investigate the molecular abundances in the protoplanetary disks with a model more realistic than the previous ones. First, we take into account the ionization of the gas by cosmic rays and the subsequent ion-molecule reactions, which are not included in the KI model. Since the attenuation length of the cosmic-ray ionization is about 96 g cm^{-2} , the disk is partially ionized by cosmic rays at $R \gtrsim 7$ AU in the minimum-mass solar nebula (Umebayashi & Nakano 1981). The reaction rate coefficients of ion-molecule reactions are larger than those of neutral-neutral reactions especially at the low temperature typical at $R \gtrsim 10$ AU. Thus, ion-molecule reactions can be efficient especially in the outer regions of the disk, regions that were regarded as chemically inactive in the KI model. The second point concerns the disk model. In this paper we adopt the standard accretion-disk model (Lynden-Bell & Pringle 1974). In the KI model they assumed that the matter in the outer regions ($R \gg 1$ AU) was transported from the region inside the quenching radius ($R < 1$ AU). However, it is implausible that most matter in the outer regions passed within the quenching radius. According to Lynden-Bell & Pringle (1974), most of the matter loses its angular momentum due to viscosity and accretes toward the central star; most of the matter migrates inward at any radius. Indeed, observations at ultraviolet, optical, and infrared wavelengths suggest that there are accretion flows in protoplanetary disks (Hartigan et al. 1991; Basri & Bertout 1993 and references therein). Stevenson (1990) investigated the efficiency of mixing in the standard accretion disk and found that the amount of contamination from inside the quenching radius is small or negligible in the outer region of the disk. Third, we investigate the molecular abundances by solving directly the time-dependent reaction equations. In contrast to the KI model, we obtain the evolution and distribution of molecular abundances fully time dependently.

Some of the points described above were taken into account in recent works on the molecular evolution of the protoplanetary disks including ours. Aikawa et al. (1997, hereafter Paper I) showed that the ionization and ion-molecule reactions play an important role in the molecular evolution. But they neglected the accretion flow in the disk. Although Finocchi & Gail (1997) took into account the effects of ionization and accretion flow, they did not consider the condensation of molecules onto grains and the effect of charged grains, which play important roles in the molecular evolution (Paper I). In this paper we take into account the effects of ionization, accretion flow, formation of ice mantles, and desorption of molecules from the ice mantles at the same time. Molecular evolution in the accretion disk was also investigated recently by Willacy et al. (1998, hereafter W98). The main difference between W98 and this paper is in the temperature distribution in the disk as mentioned in § 4.1. In this paper we also investigate dependences of molecular evolution on some physical parameters in the disk, which were not worked out in W98.

In § 2 we describe our models of accretion disk and chemical reaction network. In § 3 we show the numerical results on the evolution and distribution of molecular abundances and the dependence of our results on some physical

parameters such as the cosmic-ray flux and the grain size. Comparison with previous works (KI model and W98), the dependence of our results on the disk model, and the uncertainties in the reaction network are discussed in § 4. In § 5 we compare our results with the composition of comets, and give some expectations for the future molecular line observations of the disks based on our results.

2. MODEL

2.1. Disk Model

We describe here our theoretical model for the structure of the protoplanetary disks. The excess of ultraviolet radiation and intense H α emission lines observed for T Tauri stars indicate that the disks are accreting toward the central star at age \lesssim several $\times 10^6$ yr (Strom et al. 1989). We adopt the steady accretion disk model (Lynden-Bell & Pringle 1974; Frank, King, & Raine 1992, p. 77), in which the accretion rate and the disk structure are assumed not to change with time. The column density Σ of the disk at the radial distance R from the central star is given by

$$v\Sigma(R) = \frac{\dot{M}}{3\pi} \left[1 - \left(\frac{R_*}{R} \right)^{1/2} \right], \quad (1)$$

where v is the viscosity, \dot{M} is the mass accretion rate, and R_* is the radius of the central star; we adopt the cylindrical coordinates (R, Φ, Z) . The cause of the viscosity is not well known, though some candidates have been proposed, such as turbulence caused by the shearing instability of a weakly magnetized disk (Balbus & Hawley 1991; Hawley & Balbus 1991). Because of insufficient knowledge we adopt the α -prescription of the viscosity given by Shakura & Sunyaev (1973):

$$v = \alpha c_s H. \quad (2)$$

The sound velocity c_s and the scale height H of the disk are given by

$$c_s = \left(\frac{kT}{\mu m_H} \right)^{1/2}, \quad (3)$$

$$H = \left(\frac{2kT}{\mu m_H} \frac{R^3}{GM_*} \right)^{1/2}, \quad (4)$$

where k is the Boltzmann constant, m_H is the mass of a hydrogen atom, G is the gravitational constant, T is the temperature, μ is the mean molecular weight of the gas, and M_* is the mass of the central star. We adopt $\mu = 2.37$, $M_* = 1 M_\odot$, and $R_* = 3 R_\odot$. We determine the accretion rate \dot{M} and α by referring to the observational data. The ultraviolet excesses indicate $\dot{M} \sim 10^{-8}$ – $10^{-7} M_\odot \text{ yr}^{-1}$, which corresponds to $\alpha \sim 10^{-2}$, for the disk mass $M \sim 10^{-2} M_\odot$ estimated from the spectral energy distribution in the infrared wavelengths (Basri & Bertout 1993).

We assume for simplicity that the disk is isothermal in the Z -direction because the heat is easily transported in this direction by the thermal radiation of dust particles. Then the gas density at the midplane of the disk by number of hydrogen nuclei is given by

$$n_H = 0.706 \frac{2}{\sqrt{\pi}} \frac{\Sigma}{2Hm_H}, \quad (5)$$

for the mass fraction of hydrogen, 0.706, for the solar abundance (Anders & Grevesse 1989). The accretion velocity is

given by

$$v_R = \frac{\dot{M}}{2\pi R \Sigma}. \quad (6)$$

The temperature distribution in the disk is determined by the balance between heating by absorption of the stellar radiation and by gravitational energy release due to viscous accretion and cooling due to thermal radiation of the disk;

$$(1 - e^{-2\tau})\sigma T^4 = \frac{L_*}{4\pi R^2} \frac{1}{2} \left\{ \frac{4}{3\pi} \left(\frac{R_*}{R} \right) + R \frac{d}{dR} \left(\frac{H}{R} \right) \right\} + \frac{3GM_*\dot{M}}{8\pi R^3} \left\{ 1 - \left(\frac{R_*}{R} \right)^{1/2} \right\}, \quad (7)$$

where σ is the Stefan-Boltzmann constant, L_* is the luminosity of the central star, and

$$\tau = \kappa \Sigma \quad (8)$$

is the optical thickness of the disk for the thermal radiation, κ being the absorption coefficient. The first term on the right-hand side of equation (7) represents the heating by the central star (Kusaka, Nakano, & Hayashi 1970; Ruden & Pollack 1991), and the second term represents the energy released by viscous accretion (Lynden-Bell & Pringle 1974). The left-hand side of equation (7) represents the emission of the thermal radiation from the disk; this expression is exact when $\tau \ll 1$ and holds well at $\tau \gtrsim 1$. We adopt the absorption coefficient

$$\kappa = 0.5 \left(\frac{T}{30 \text{ K}} \right)^2 \text{ cm}^2 \text{ g}^{-1} \quad (9)$$

according to Krügel & Siebenmorgen (1994), who calculated the absorption coefficient for various kinds of dust particles using Mie theory. We adopt $L_* = 1 L_\odot$ in this paper.

The structure of the accreting protoplanetary disk is obtained by solving equations (1)–(9). Adopting $\dot{M} = 1 \times 10^{-8} M_\odot \text{ yr}^{-1}$, $\alpha = 0.01$, and $L_* = 1 L_\odot$, we obtain the temperature distribution as shown by the solid line in Figure 1a. In the region of radius $R \gtrsim 10$ AU, which we are primarily concerned in (see below), the energy released by accretion is much smaller than the radiation energy from the central star, and thus the first term dominates in the right-hand side of equation (7). This ensures the isothermality of the disk in the Z -direction assumed above even if the disk is optically thick to its own thermal radiation. Then the temperature is nearly proportional to $R^{-3/7}$ as long as the disk is optically thick to the thermal radiation in accordance with Kusaka et al. (1970). At larger radii, $R \gtrsim 100$ AU, where the disk is optically thin to the thermal radiation, the temperature is almost independent of R . Although energy flux from the central star decreases with radius in proportion to R^{-2} , it is compensated by decrease of disk opacity for thermal radiation and flaring of the disk.

The dotted line in Figure 1a shows the distribution of the column density Σ . The column density is proportional to $R^{-15/14}$ at $R \lesssim 10$ AU, where the disk is optically thick to the thermal radiation, while it is proportional to $R^{-3/2}$ at $R \gtrsim 100$ AU, where the disk is optically thin. It is to be noted that the disk is mainly ionized by cosmic rays at $R \gtrsim 2$ AU, where Σ is smaller than the attenuation length of

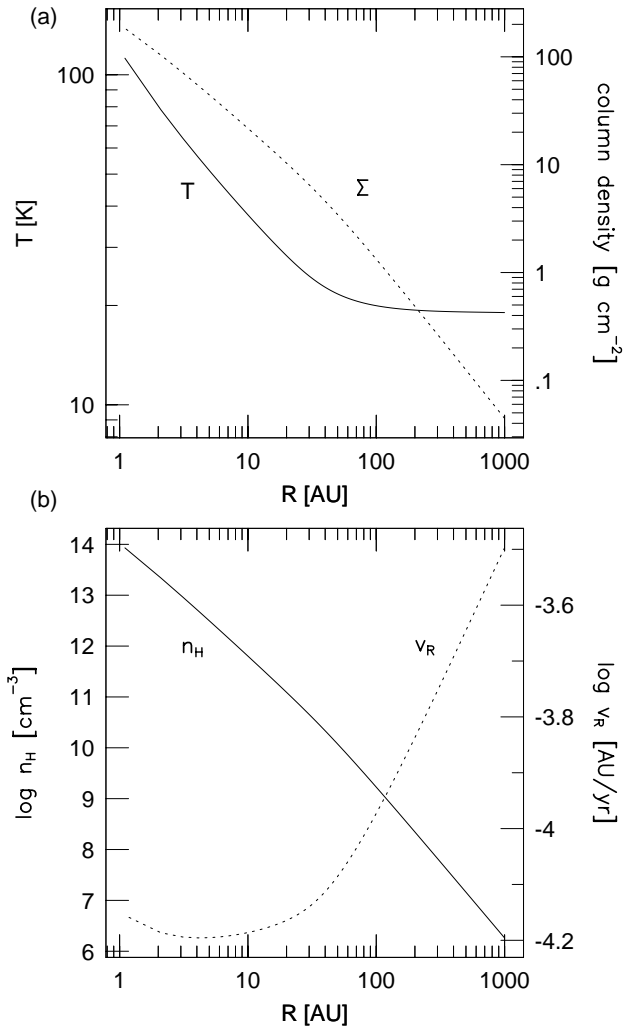


FIG. 1.—Model of the disk in steady accretion with the accretion rate $\dot{M} = 1 \times 10^{-8} M_{\odot} \text{ yr}^{-1}$ and the coefficient for viscosity $\alpha = 0.01$ exposed to the stellar radiation of $L_{*} = 1 L_{\odot}$; (a) distribution of the temperature T (solid line) and the column density Σ (dotted line), and (b) distribution of the gas density by number of hydrogen nuclei, n_H (solid line), and the accretion velocity v_R (dotted line).

cosmic-ray ionization, 96 g cm^{-2} (Umebayashi & Nakano 1981). Thus, the ionization by cosmic rays should be taken into account in this region.

Figure 1b shows the gas density by number of hydrogen nuclei n_H (solid line) and the accretion velocity v_R (dotted line) in the disk. The matter migrates $\sim 10^2 \text{ AU}$ in 10^6 yr .

2.2. Reaction Network

Because density and temperature may not be high enough for the chemical equilibrium to be achieved within the evolutionary timescale of the protoplanetary disk, it will be necessary to solve the time-dependent reaction equations to find out the molecular abundances in the disk. We also consider the effect of the accretion flow. The time variation of the number density $n(i)$ of species i along the accretion flow is governed by

$$\frac{dn(i)}{dt} \equiv \frac{\partial n(i)}{\partial t} + v_R \frac{\partial n(i)}{\partial R} = S(i) - \frac{n(i)}{HR} \frac{\partial}{\partial R} (HRv_R), \quad (10)$$

where t is the time and the source term $S(i)$ is given by

$$S(i) = \sum_j \alpha_{ij} n(j) + \sum_{j,k} \beta_{ijk} n(j)n(k) + \sum_{j,k,l} \gamma_{ijkl} n(j)n(k)n(l). \quad (11)$$

The first term on the right-hand side of equation (11) represents the reactions with external particles such as ionization by cosmic rays. The second term represents the two-body reactions in which species i is formed by the reaction of species j and k , and species i ($=j$) is destroyed by the reaction with k . The third term represents the three-body reactions, in which species i is formed by the reaction of species j and k with the excess energy carried away by species l . The adopted rate coefficients in the gas phase are essentially the same as those in the UMIST94 database (Millar et al. 1991; Farquhar & Millar 1993). We also take into account some three-body reactions referring to the reaction network adopted in the atmospheric chemistry (Brasseur & Solomon 1986).

The total number of species and that of reactions included in our network are about 250 and 2300, respectively.

Because of the poor experimental data and theoretical study, we have insufficient information on the rate coefficients of three-body reactions. Thus, we consider only the regions of density, $n_H \lesssim 10^{12} \text{ cm}^{-3}$, which corresponds to $R \gtrsim 10 \text{ AU}$ in our disk model (Fig. 1b). With a typical rate coefficient $k \sim 10^{-30} \text{ cm}^6 \text{ s}^{-1}$ for three-body reactions, we have $kn(\text{H}_2) \lesssim 10^{-18} \text{ cm}^3 \text{ s}^{-1}$ in this density range even for the most abundant species H_2 as a third body. This value is smaller than the characteristic rate coefficient $\sim 10^{-17} \text{ cm}^3 \text{ s}^{-1}$ for the radiative association, which is the slowest among the two-body reactions. Thus, three-body reactions are not important in this density range.

The attenuation length of cosmic-ray ionization, 96 g cm^{-2} (Umebayashi & Nakano 1981), is much larger than the column density of the disk at $R \gtrsim 10 \text{ AU}$. Thus, we adopt the “standard” ionization rate for the molecular clouds, $\zeta = 1.3 \times 10^{-17} \text{ s}^{-1}$, which has been derived from the observed abundances of ions in molecular clouds (Lepp 1992). This is not much different from the ionization rate calculated from the observed cosmic-ray intensity (Spitzer & Tomasko 1968). Although we take into account the ionization and dissociation of molecules by the interstellar and stellar ultraviolet radiation, they have been found to hardly affect the results; the ultraviolet radiation is attenuated by grains in a thin surface layer of the disk with a thickness $\sim 10^{-3} \text{ g cm}^{-2}$.

In addition to the reactions in the gas phase, we also take into account the reactions on grain surfaces: formation of H_2 molecules, recombination of ions and electrons, as well as formation of ice mantles due to adsorption of molecules and thermal desorption of molecules from the ice mantles. For simplicity and clarity, we do not consider the other chemical reactions on grain surfaces because detailed mechanisms and reaction rate coefficients are not well known. We adopt the same adsorption and desorption rate coefficients as in Paper I (see also Yamamoto, Nakagawa, & Fukui 1983; Hasegawa & Herbst 1993; Sandford & Allamandola 1993). We neglect the nonthermal desorption induced by cosmic rays, UV photons, and X-rays because they are not effective in the density region we are concerned in. Owing to the high density, the adsorption rate in the

TABLE 1
THE ABUNDANCES OF ELEMENTS^a AND GRAINS

Element	Abundance	Element	Abundance
H	1.00	Mg	1.09(-6)
He	9.75(-2) ^b	Si	9.74(-7)
C	7.86(-5)	S	9.14(-6)
N	2.47(-5)	Fe	2.74(-7)
O	1.80(-4)	Grain	1.02(-2) ^c
Na	2.25(-7)		

^a The abundances by number of the elements that are in the gas phase and in grain mantles. The elements in refractory grain cores are not included.

^b $a(b)$ means $a \times 10^b$.

^c The abundance of refractory grain cores by mass relative to hydrogen.

disk is much higher than in molecular clouds, where non-thermal desorption can be effective (Aikawa et al. 1996, Bergin & Langer 1997).

We determine the initial abundances of various molecules and dust in the following way. We adopt the solar abundance (Anders & Grevesse 1989) as the total elemental abundances. Considerable amounts of elements, except for hydrogen and helium, are in refractory dust cores. Since the dust cores do not evaporate at the temperatures with which we are concerned ($T \lesssim 100$ K), we exclude the elements taken in the cores from the scheme of chemical reactions. The amount of the elements that are not in the dust cores and participate in the reactions can be estimated from the observations of the diffuse medium (e.g., Morton 1974) and is shown in Table 1.

We assume for simplicity that all grains are spherical with radius $a = 10^{-5}$ cm and their internal density $\rho_g = 2.5$ g cm⁻³, typical values for the interstellar grains. Thus, we find the relative number density of grains $n(\text{grain})/n_{\text{H}} = 1.63 \times 10^{-12}$. We neglect the increase of grain radius due to the growth of the ice mantle because this is not very large.

We determine the initial molecular abundances of the protoplanetary disks referring to the abundances of the molecular clouds, which are raw material of the protoplanetary disks. We assume that initially hydrogen is in the form of H₂, carbon is in CO, the remaining oxygen is locked up as water ice mantle, nitrogen is in the form of N₂, and the other heavy elements are in atomic forms. We call this case Model A. The dependence of our results on the initial molecular abundances will be discussed in § 3.3.

3. NUMERICAL RESULTS

3.1. Molecular Evolution in the Accreting Flow

In this section we show the results of the numerical calculations on the molecular evolution. We first describe the molecular evolution of the matter that is accreting toward the central star. We consider the disk, which initially has a radius $R \sim 1000$ AU. The matter at each radius migrates inward with the velocity v_R given by equation (6). The density n_{H} and the temperature T of the matter change with time according to equations (5) and (7), respectively, as the matter migrates toward the central star. We solve equations (10) and (11) along the accretion flow. The calculation is performed for a period of 3×10^6 yr, which is a typical duration time of the accretion phase (Strom et al. 1989).

As an example we show the evolution of molecular abundances in the matter, which migrates from $R = 395$ AU to

$R = 10$ AU in 3×10^6 yr. Figures 2a–2e show the evolution up to $t = 2.4 \times 10^6$ yr, while the temperature of the matter is kept almost constant. In this period the matter migrates down to $R = 54$ AU. Figure 2a shows the density and temperature of the matter as a function of time, or along the path of migration.

Figures 2b–2e show the evolution of C-, N-, O-, and S-bearing molecules, respectively. Since the temperature is almost constant at $T \sim 20$ K, the evolution is very similar to those described in Paper I.

Initially, all carbon is assumed to be in the form of CO. As time goes on, CO₂ ice, HCN ice, CH₄ ice, and H₂CO ice form as shown in Figure 2b. The main formation processes of these molecules in the gas phase are shown in Figure 3a. First, some of H₂ molecules are ionized by cosmic rays to produce H₂⁺ ions, which subsequently react with H₂ to form H₃⁺. By reaction with H₃⁺, CO is transformed into HCO⁺, some of which become HCO through grain-surface recombination. Finally, reactions of HCO with O and N form CO₂ and HCN, respectively. Although neither O nor N atoms exist initially, they are formed from CO and N₂, respectively, through ion-molecule reactions. The reaction of HCO with HCO produces H₂CO. Helium ions, He⁺, which are formed by cosmic-ray ionization, react with CO to form C⁺. Radiative association with H₂ and H-atom abstraction from H₂ transform C⁺ into CH₅⁺, which recombines to form CH₄.

Owing to the low temperature and high density, most of these products are adsorbed onto grain surfaces in a short timescale $\sim 10^3(10^7 \text{ cm}^{-3}/n_{\text{H}})$ yr and accumulate in ice mantles. Formation of ice mantles works as a “sink” in the chemical reaction network. Some kinds of species can survive by forming ice mantles; otherwise they are destroyed and transformed into other molecules by the reactions in the gas phase. For example, CH₄ reacts with C⁺ to form larger hydrocarbons at higher temperatures at which CH₄ is easily desorbed from the ice mantles (see below).

Figure 2c shows the time variation of the abundance of N-bearing molecules relative to hydrogen. Initially, all nitrogen is assumed to be in the form of N₂. As time goes on, HCN ice and NH₃ ice become dominant. The main formation process of NH₃ is as follows (Fig. 3b). The reaction of N₂ with He⁺ forms N⁺, which is transformed into NH₄⁺ by repeated H-atom abstraction from H₂; NH₄⁺ is turned into NH₃ through dissociative recombination, which finally accumulates in the ice mantle. As described above, HCN is formed through the reaction of HCO with N atom. Nitric oxide NO is mainly formed by the reactions $\text{N} + \text{OH} \rightarrow \text{NO} + \text{H}$ and $\text{O} + \text{NH} \rightarrow \text{NO} + \text{H}$. The reaction of HCN with HCO⁺ produces HCNH⁺, which recombines to form CN.

Figure 2d shows the time variation of the abundance of O-bearing molecules. Initially, oxygen is assumed to be in the form of H₂O ice and CO. As shown in Figure 3c, the reaction with He⁺ destroys CO to form an O atom, which reacts with HCO to produce OH. The oxygen molecule O₂ is formed by the reaction of OH with an O atom.

Figure 2e shows the time variation of the abundance of S-bearing molecules. Initially, sulphur is assumed to be in atomic form. As time goes on, OCS ice, SO ice, and H₂S ice are formed. As shown in Figure 3d, radiative association of CO with S forms OCS. Reaction of S with OH produces SO, which reacts with O to form SO₂. Sulphur monoxide

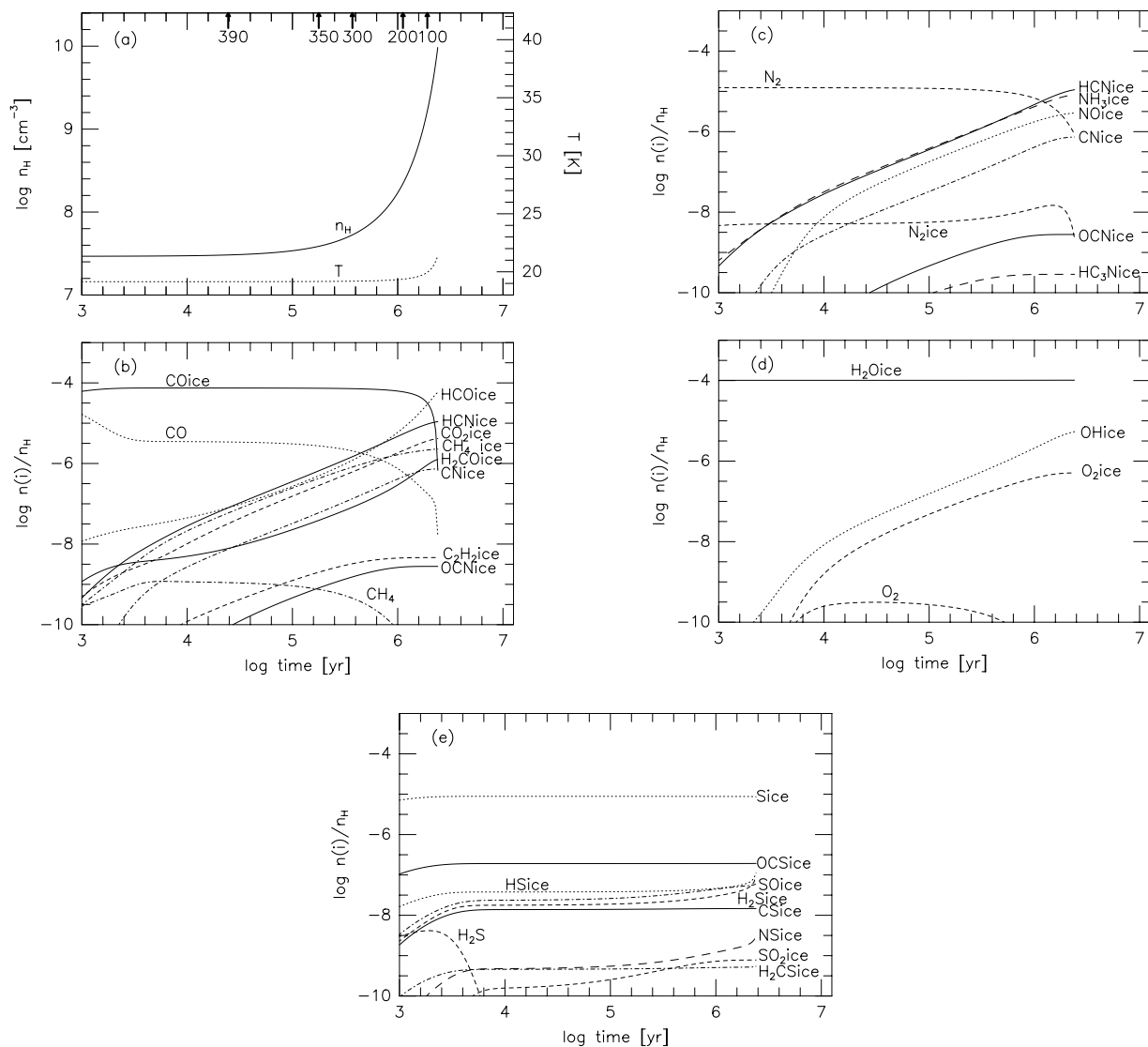


FIG. 2.—Evolution of molecular abundances in the matter which migrates from $R = 395 \text{ AU}$ to $R = 54 \text{ AU}$ in $2.4 \times 10^6 \text{ yr}$; (a) the temperature T (dotted line) and the density of the matter, n_H (solid line), as functions of time, and (b)–(e) evolution of C-, N-, O-, and S-bearing molecules, respectively. The numerals with arrows in (a) show the distances of the matter from the central star in units of AU at the corresponding times.

SO also reacts with C to form CS. Sulphur atoms react with H_3^+ or HCO^+ to form HS^+ , which is transformed to H_3S^+ by radiative association with H_2 . Then, H_2S is formed by dissociative recombination of H_3S^+ .

Since the evolution at the later stages $t \geq 2.4 \times 10^6 \text{ yr}$ is complicated, it is shown separately in Figures 4a–4e with the time (abscissa) in the linear scale. Figure 4a shows the density and the temperature of the matter as functions of time. In this period the matter migrates from 54 to 10 AU, and the temperature rises rapidly up to $T \approx 38 \text{ K}$. As the matter moves to warmer regions, some ices sublime. For example, CH_4 is desorbed at $t \sim 2.9 \times 10^6 \text{ yr}$ ($R \sim 20 \text{ AU}$) when the temperature rises to its sublimation temperature $\sim 28 \text{ K}$. Then CH_4 is transformed into larger hydrocarbons C_2H_2 , C_3H_4 , etc., by ion-molecule reactions and dissociative recombinations in the gas phase (Fig. 3a). The abundance of CO in the gas phase shows a complex behavior. Its abundance is decreasing at $t \sim 2.4 \times 10^6 \text{ yr}$ ($R \sim 50 \text{ AU}$) as CO is transformed into the other C-bearing molecules such as H_2CO and CO_2 . At $t \sim 2.9 \times 10^6 \text{ yr}$ ($R \sim 20 \text{ AU}$), CO is formed anew from radicals such as HCO and OH, which

have been desorbed from the ice mantle. Carbon monoxide is also produced from CH_3 , which has been formed from CH_4 . Formaldehyde H_2CO is produced by the reaction $\text{HCO} + \text{HCO} \rightarrow \text{H}_2\text{CO} + \text{CO}$ at $t \sim 2.9 \times 10^6 \text{ yr}$. Similarly, OCN ice, NO_2 ice, and H_2CS ice begin to increase rapidly when their precursors CN, NO, and S, respectively, start sublimating.

3.2. Spatial Distribution of Molecules in the Disk

To find out the spatial distribution of the molecular abundances in the accretion disk at $t = 3.0 \times 10^6 \text{ yr}$, we perform the similar calculation as described above for the matter which starts migration at various positions; the matter moving in $3.0 \times 10^6 \text{ yr}$ from $R = 426$ to 20 AU, 456 to 30 AU, 486 to 40 AU, 514 to 50 AU, 541 to 60 AU, 568 to 70 AU, and 619 to 90 AU.

Figures 5a–5d show the spatial distribution of C-, N-, O-, and S-bearing molecules, respectively, at $t = 3.0 \times 10^6 \text{ yr}$. We can see that the molecular abundances do not change much at $R \geq 50 \text{ AU}$, where the temperature is nearly constant at $\sim 20 \text{ K}$. This is because the molecular evolution

does not depend sensitively on the density, though it depends crucially on the temperature. At $R \lesssim 50$ AU, the temperature rises considerably as R decreases, and therefore molecular abundances vary with radius. For example, CH_4 ice is much less abundant at $R \lesssim 20$ AU than in the outer regions. Instead, larger hydrocarbons such as C_3H_4 ice, which are formed from the desorbed CH_4 , are more abundant at $R \lesssim 20$ AU than in the outer regions.

At $R \lesssim 20$ AU, HCO cannot accumulate in the ice mantle. Therefore, H_2CO and HCN , which are produced from HCO , are more abundant than in the outer regions. On the other hand, the abundance of NH_3 ice is constant at $R = 10\text{--}90$ AU, since the temperature in this region is much lower than the sublimation temperature of NH_3 (~ 80 K) and higher than the sublimation temperature of the precursor molecule N_2 (~ 20 K).

In the region of $20 \text{ AU} \lesssim R \lesssim 40 \text{ AU}$, CO is significantly depleted because it is destroyed by the reaction with H_3^+ in the gas phase. At $R \lesssim 20$ AU the abundance of CO is high

once again as it is produced from HCO , which is desorbed from ice mantles.

Figure 6 shows the distribution of molecular abundances at an earlier stage $t = 1 \times 10^6$ yr. To get this figure we followed the molecular evolution in the matter which migrates in 1×10^6 yr from 91 to 10 AU, 107 to 20 AU, 123 to 30 AU, 139 to 40 AU, 155 to 50 AU, 171 to 60 AU, 186 to 70 AU, and 216 to 90 AU. Many species such as hydrocarbons, NH_3 , and SO have already been formed at this time. Comparing Figure 6 with Figure 5, we can see that the abundances of these species increase with time anywhere in the disk, while CO and N_2 decrease with time anywhere.

3.3. Dependence on the Parameters

3.3.1. Ionization Rate

In the previous subsections we discussed how ionization by cosmic rays drives the molecular evolution, especially in the outer regions of the protoplanetary disks. Since the attenuation length of cosmic-ray ionization, 96 g cm^{-2} , is

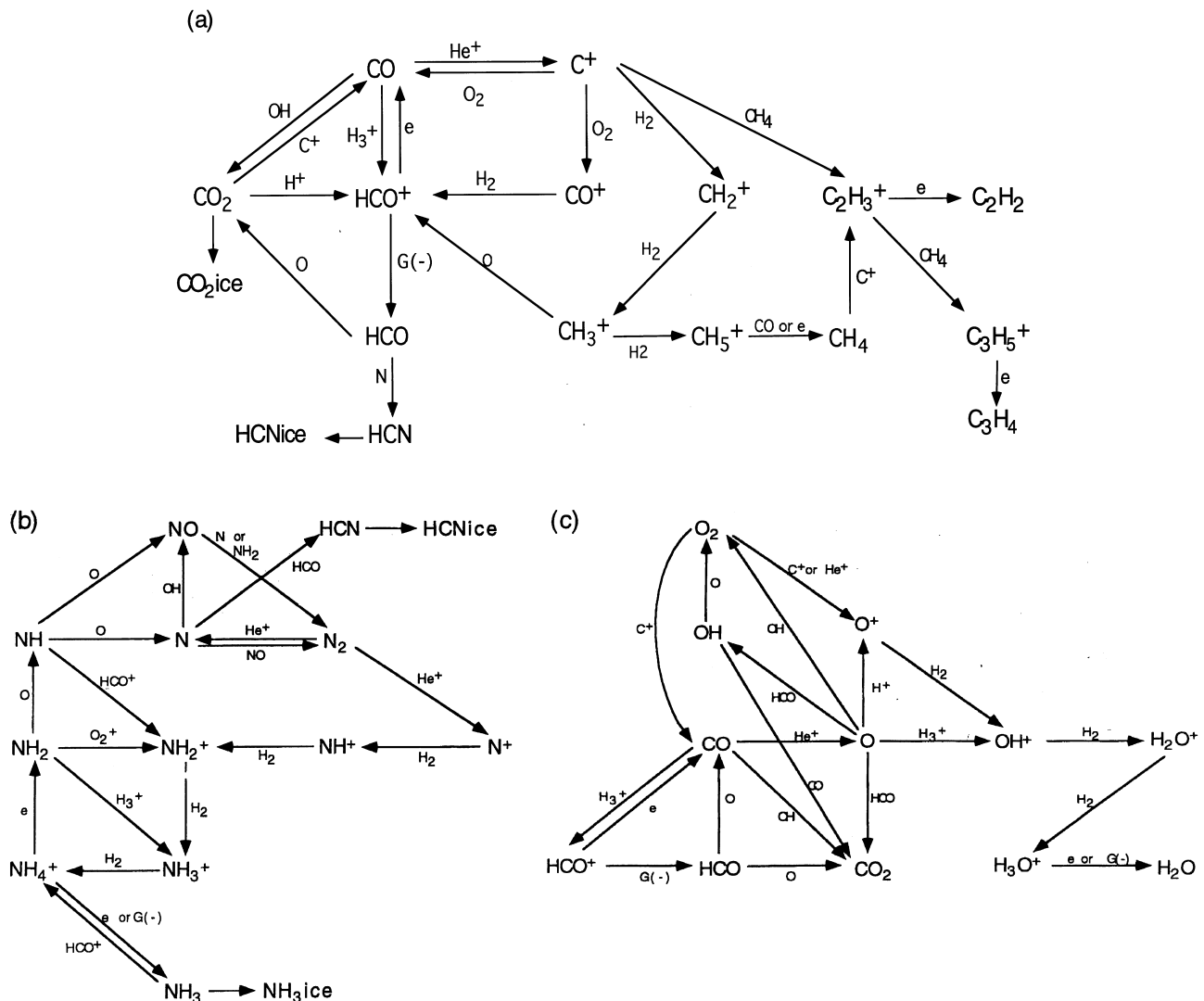


FIG. 3.—Major reactions concerning (a) carbon, (b) nitrogen, (c) oxygen, and (d) sulphur compounds. The grain-surface recombinations are shown by the arrows with “G(−)”.

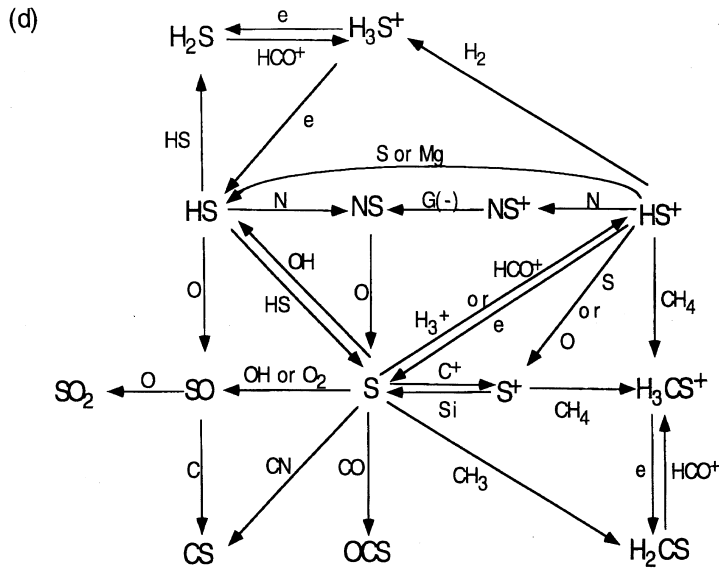


FIG. 3.—Continued

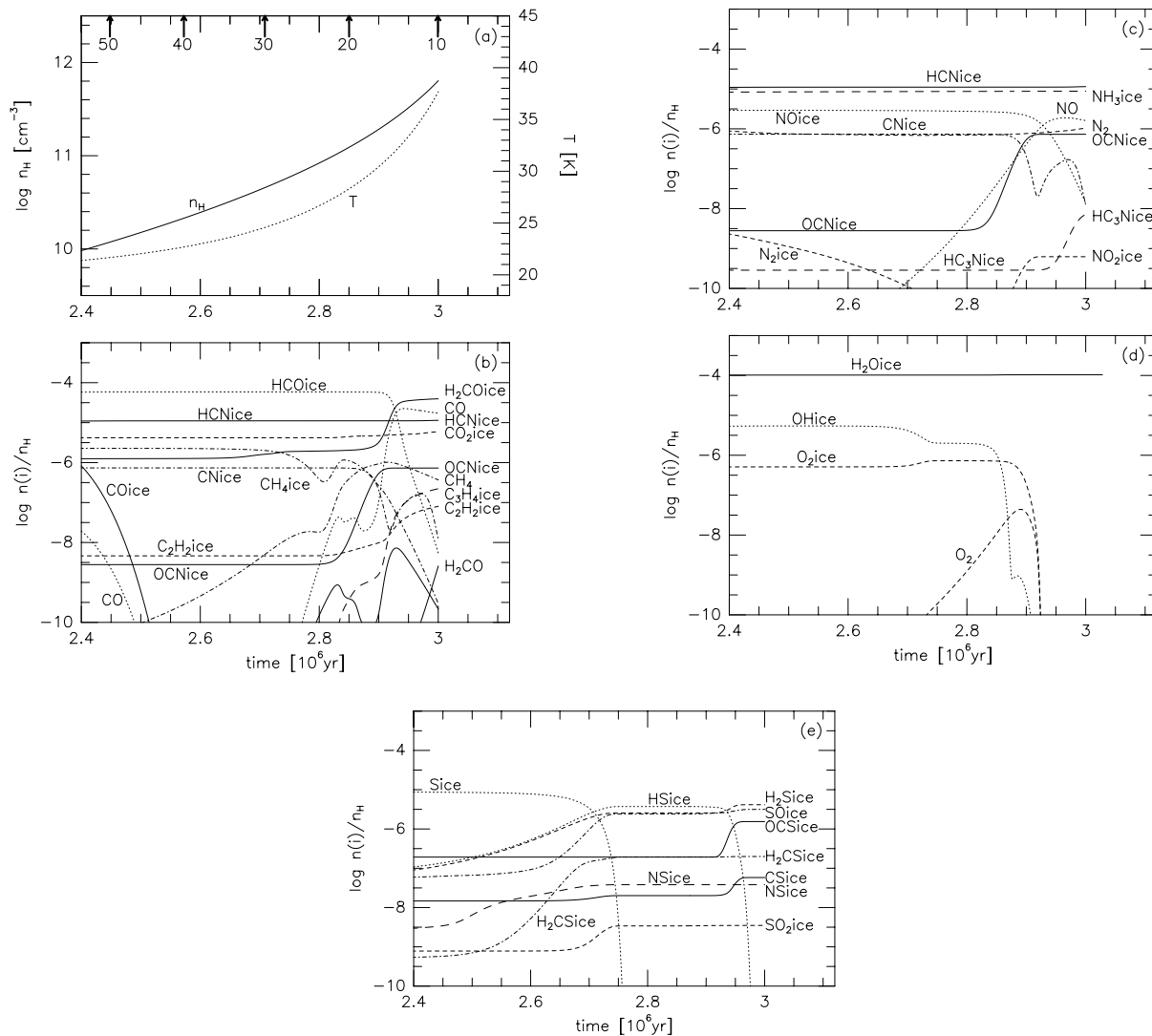


FIG. 4.—Evolution of molecular abundances in the matter which migrates from $R = 54$ AU to $R = 10$ AU in the period between $t = 2.4 \times 10^6$ and 3×10^6 yr (after the final stage of Fig. 2); (a) the temperature T (dotted line) and the density of the matter, n_{H} , (solid line) as functions of time, and (b)–(e) evolution of C-, N-, O-, and S-bearing molecules, respectively. The numerals with arrows in (a) show the distances from the central star in units of AU at the corresponding times.

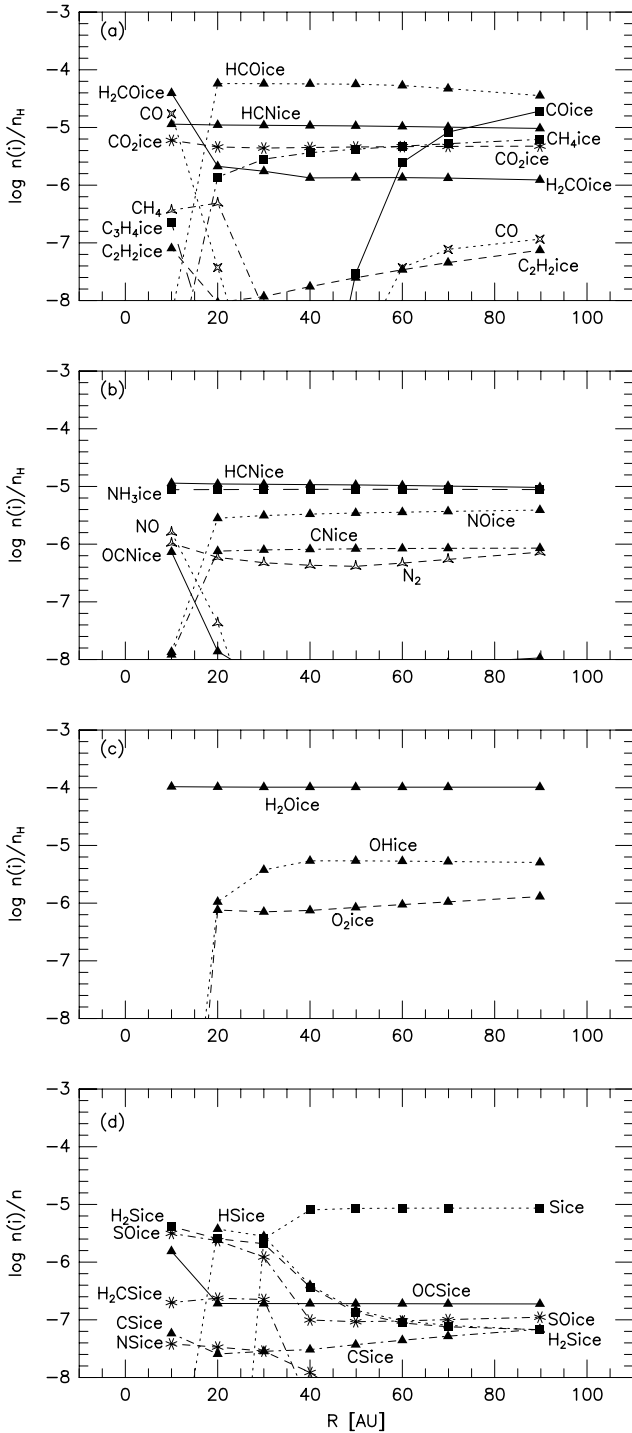


FIG. 5.—Distribution of molecular abundances in the accretion disk at $t = 3 \times 10^6$ yr. Panels (a)–(d) show the distribution of C-, N-, O-, and S-bearing molecules, respectively.

significantly larger than the column density of the disk at $R \gtrsim 10$ AU, we adopted the ionization rate appropriate to the molecular clouds, $\zeta = 1.3 \times 10^{-17} \text{ s}^{-1}$. However, there are some uncertainties about the ionization rate in the protoplanetary disks; (i) low-energy cosmic rays may be scattered by strong magnetized protostellar winds; (ii) cosmic rays can be scattered by the magnetic fields in the turbulent disk (Dolginov & Stepinski 1994); and (iii) the flux of cosmic rays can be significantly larger if the protostar is located near a young supernova remnant.

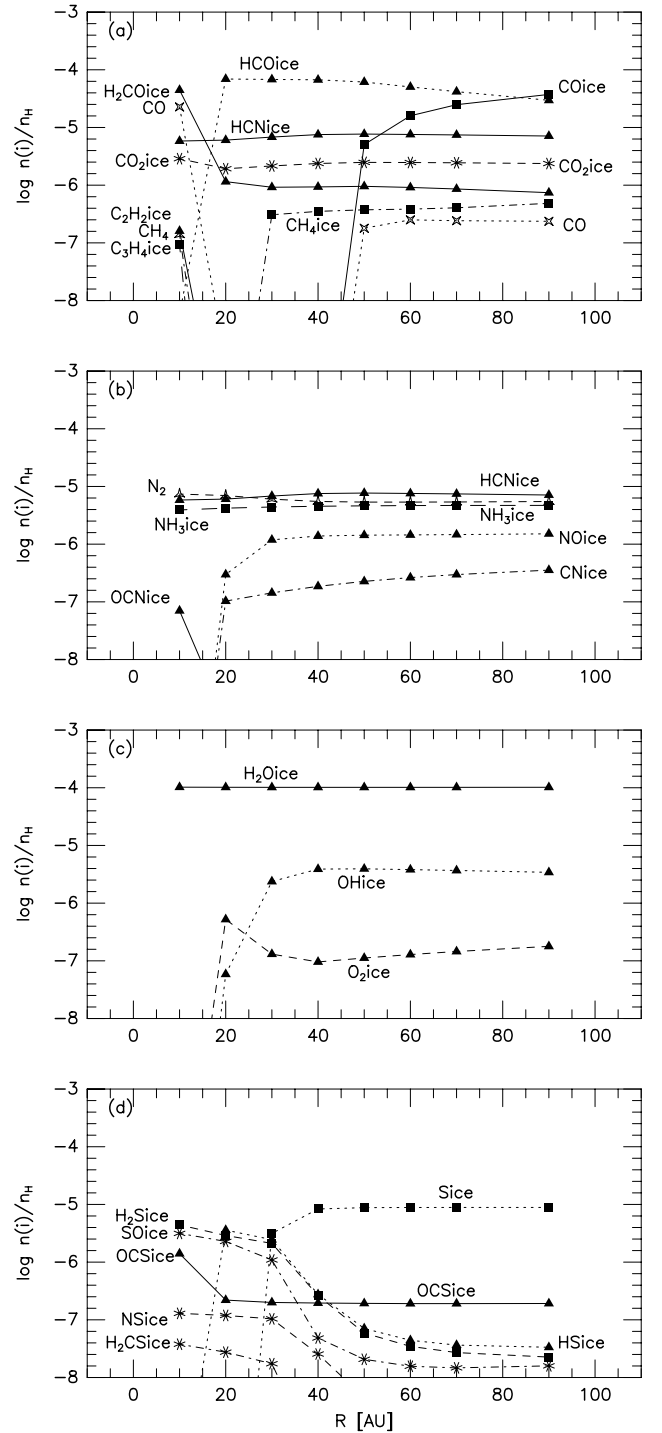


FIG. 6.—Distribution of molecular abundances in the same accretion disk as in Fig. 5, but at an earlier stage $t = 1 \times 10^6$ yr. The other details are the same as in Fig. 5

Although the precise value strongly depends on the physical situation around young stellar objects, the ionization by cosmic rays can be as low as $\zeta \sim 10^{-18} \text{ s}^{-1}$ if the flux of cosmic rays at energy below 100 MeV are scattered completely (Umebayashi & Nakano 1981). Dolginov & Stepinski (1994) investigated the propagation of cosmic rays within a magnetized turbulent disk and found that the ionization rate is proportional to $\exp[-(d/d_{\text{diff}})^2]$, where d is the vertical distance measured from the disk surface and a penetration depth d_{diff} is 0.2 to 0.3 times the scale height H

of the disk. Though their disk model is quite different from ours, it may be possible that the ionization rate by cosmic rays is decreased extensively and the ionization due to decay of radioactive elements becomes dominant. For the solar abundance, the most efficient element is ^{40}K , which gives the total ionization rate of $\sim 10^{-22} \text{ s}^{-1}$ (Umebayashi & Nakano 1981). The evidence for extinct ^{26}Al in the Allende meteorite suggests that the solar system was formed near a supernova remnant (Clayton 1985). Since supernovae are considered to be sources of cosmic rays, the ionization rate in the solar nebula might have been by at least an order of magnitude higher than that adopted above. Such a high value is suggested from the heating of interstellar matter (Hayakawa, Nishimura, & Takayanagi 1961). In addition to cosmic rays, the universal existence of gamma ray emission from the decay of ^{26}Al in our galaxy (Mahoney et al. 1984; Share et al. 1985; Diehl et al. 1993) suggests that ^{26}Al can be an important source of ionization. If ^{26}Al were present with the abundance estimated from the amount of ^{26}Mg in the Allende refractory inclusions, the ionization rates reach about several $\times 10^{-19} \text{ s}^{-1}$ (Umebayashi & Nakano 1981; T. Umebayashi 1997, private communication). Because of these uncertainties, we have also investigated the cases of $\zeta = 1.3 \times 10^{-18} \text{ s}^{-1}$ and $1.3 \times 10^{-16} \text{ s}^{-1}$.

In Figure 7 we show the evolution of molecular abundances in the matter which migrates from $R = 568$ to 70 AU in $3 \times 10^6 \text{ yr}$ for the three cases of the ionization rate ζ ; (a) $1.3 \times 10^{-18} \text{ s}^{-1}$, (b) $1.3 \times 10^{-17} \text{ s}^{-1}$, and (c) $1.3 \times 10^{-16} \text{ s}^{-1}$. We can see that the molecular evolution is critically dependent on the ionization rate. The abundances of species such as CO_2 ice, CH_4 ice, NH_3 ice, and H_2S ice at $t = 3 \times 10^6 \text{ yr}$ are lower by a factor of 3–10 for the case of the low ionization rate (Fig. 7a) compared with the standard case (Fig. 7b). The formation of these molecules starts by the reactions of CO , N_2 , and S with He^+ and H_3^+ . Since the production rates of He^+ and H_3^+ are proportional to the ionization rate, the formation of CO_2 ice, CH_4 ice, NH_3 ice, and H_2S ice is more efficient in the case of higher ionization rate. However, the formation rates of these molecules are not necessarily proportional to ζ because the higher formation rates are somewhat compensated by their higher

destruction rates due to radicals and ions, which are more abundant in the case of higher ionization rate.

In the case of the higher ionization rate (Fig. 7c), the abundances of CH_4 ice, hydrocarbon ice, NH_3 ice, and H_2S ice are significantly higher than those in the standard case (Fig. 7b), while the abundances of CO_2 ice and HCN ice are not. The relatively low abundances of CO_2 and HCN ices in Figure 7c can be explained as follows. These molecules are formed from HCO , which is produced via the grain-surface recombination of HCO^+ . Although HCO^+ is formed efficiently through the reaction of CO with H_3^+ because of the higher abundance of H_3^+ , HCO^+ is efficiently transformed back to CO by dissociative recombination because the abundance of electrons is also higher in the case of the higher ionization rate (Fig. 7c).

The ionization rate $\zeta \sim 10^{-18} \text{ s}^{-1}$ is probably a lower limit for the protoplanetary disks; the observed cosmic-ray flux at the energy $E \gtrsim 1 \text{ GeV}$ can provide this rate (Umebayashi & Nakano 1981 and references therein). In the case of solar nebula, the amount of ^{26}Mg in the Allende refractory inclusions also suggests this rate. For this lower limit, CH_4 , CO_2 , HCN , and NH_3 ices have the relative abundances $n(i)/n_{\text{H}} \sim 10^{-6}$ at $t = 3 \times 10^6 \text{ yr}$, and CO ice is the dominant species among C-bearing molecules with $n(\text{CO})/n_{\text{H}} \sim 10^{-4}$.

Since the ionization rate is such a critical parameter for the evolution of molecular abundances in the disk, it is desirable to estimate it by, e.g., observing the ions in the protoplanetary disks.

3.3.2. Effect of Grain Growth

So far we have assumed for simplicity that the dust/grain ratio by mass is 1.02×10^{-2} and the grain radius is 10^{-5} cm , which are typical for the interstellar grains (e.g., Mathis, Rumpl, & Nordsieck 1977). However, these parameters may change as the dust grains coagulate and/or sediment toward the midplane of the disk. We now investigate the effect of their growth and sedimentation on the molecular evolution of the disk.

Figure 8 shows the molecular evolution of the matter which migrates from $R = 568$ to 70 AU in $3 \times 10^6 \text{ yr}$ for the three cases of the grain radius a ; (a) 10^{-5} cm , (b) 10^{-4} cm ,

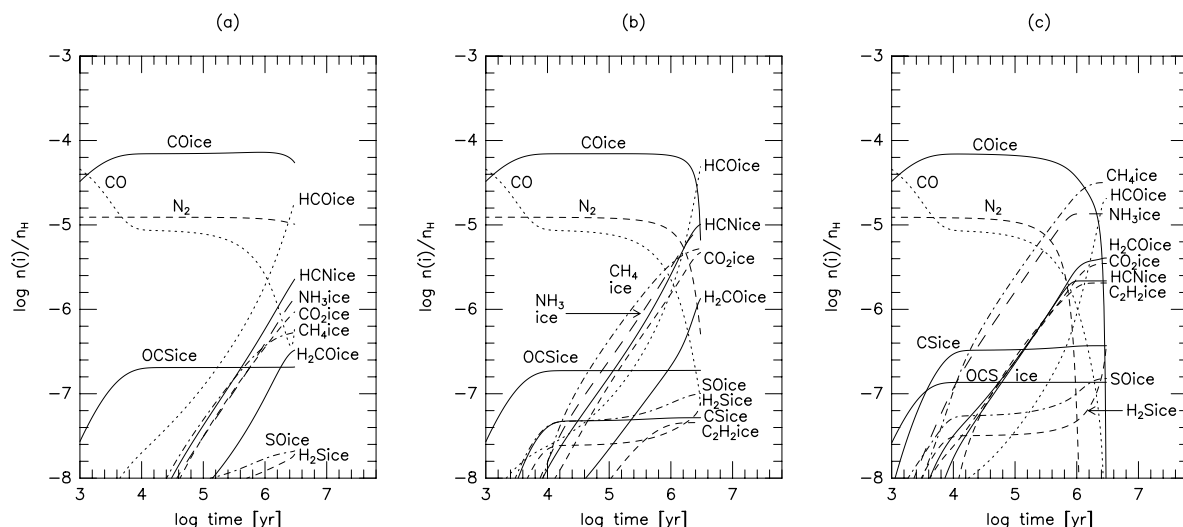


FIG. 7.—Evolution of molecular abundances in the matter which migrates from $R = 568$ to 70 AU in $3 \times 10^6 \text{ yr}$ for different values of the cosmic-ray ionization rate; (a) $1.3 \times 10^{-18} \text{ s}^{-1}$, (b) $1.3 \times 10^{-17} \text{ s}^{-1}$ (standard case), and (c) $1.3 \times 10^{-16} \text{ s}^{-1}$.

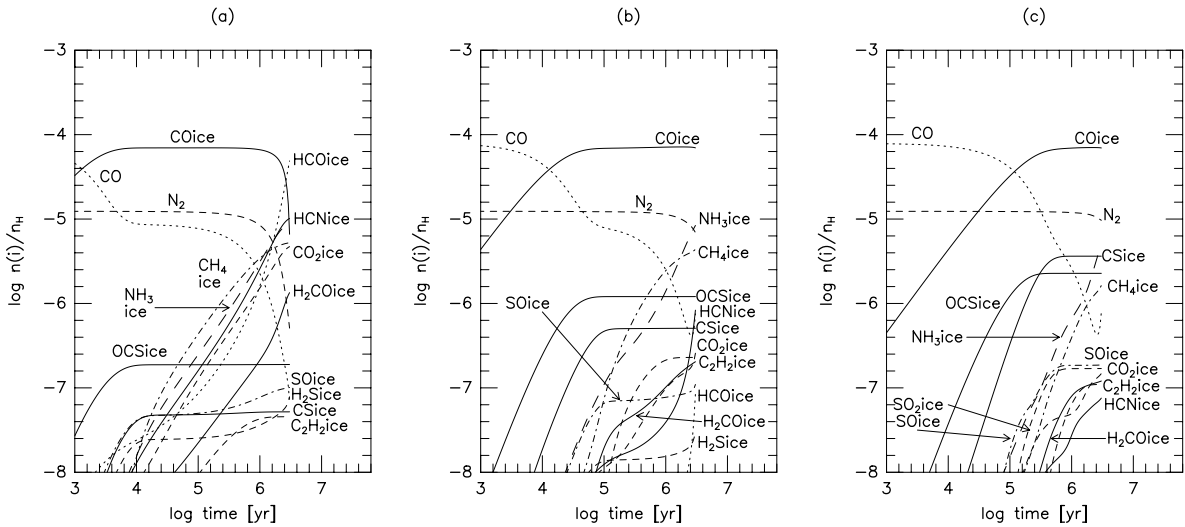


FIG. 8.—Evolution of molecular abundances in the matter which migrates from $R = 568$ to 70 AU in 3×10^6 yr for different values of the grain radius; (a) 1×10^{-5} cm (standard case), (b) 1×10^{-4} cm, and (c) 1×10^{-3} cm.

and (c) 10^{-3} cm. The dust/gas ratio by mass is fixed at the above-mentioned value. In the cases of larger (and therefore fewer) grains (Figs. 8b and 8c), the abundances of CO_2 ice, H_2CO ice, and HCN ice are lower by 1 to 2 orders of magnitude at $t = 3 \times 10^6$ yr compared with the standard case (Fig. 8a). The reason for this is that their abundances depend critically on the rate of the grain-surface recombination of HCO^+ , which is significantly smaller in the cases of larger grains; the total geometrical cross section of grains in a unit volume, $\pi a^2 n(\text{grain})$, is inversely proportional to the grain radius a . Moreover, the Coulomb force at the grain surface, which attracts ions, is smaller for larger grains. On the other hand, the abundances of CH_4 ice and NH_3 ice at $t = 3 \times 10^6$ yr are similar for the cases of $a = 10^{-5}$ cm and $a = 10^{-4}$ cm and smaller by a factor of ~ 3 for the case of $a = 10^{-3}$ cm. The adsorption rate is proportional to the total cross section of grains in a unit volume and is smaller by 2 orders of magnitude in Figure 8c compared with Figure 8a. Therefore, in the case of larger grains, higher fractions of CH_4 and NH_3 in the gas phase can be destroyed and transformed into the other molecules before they are adsorbed onto grains. Sulphur dioxide, SO_2 , on the other hand, is more abundant in the case of larger grains. For larger grains, more O_2 can be in the gas phase because of less efficient adsorption. Thus, O_2 reacts with S to form SO, which is transformed to SO_2 by the reaction with an O atom. Formation of OCS is also more efficient in the case of larger grains because there is more CO in the gas phase.

The micron-sized grains have a thermal (Brownian) velocity distribution because they couple efficiently with the smallest scales of turbulence (Weidenschilling & Cuzzi 1993; Chokshi, Tielens, & Hollenbach 1993). Therefore, the timescale of grain-grain collision in the disk is given by

$$\begin{aligned} \tau_{\text{col(th)}} &= \{\pi a^2 v_{\text{gr}} n(\text{grain})\}^{-1} \\ &= 7.6 \times 10^5 \left(\frac{20 \text{ K}}{T}\right)^{1/2} \left(\frac{a}{10^{-5} \text{ cm}}\right)^{5/2} \\ &\quad \times \left(\frac{0.0102}{\xi}\right) \left(\frac{10^8 \text{ cm}^{-3}}{n_{\text{H}}}\right) \text{ yr}, \end{aligned} \quad (12)$$

where v_{gr} is the thermal velocity of grains, ξ is the dust/gas ratio by mass, and the gas density n_{H} is normalized to the density 10^8 cm^{-3} at $R \sim 200$ AU in our disk model. Matter which is in the region of radius $R = 10$ – 90 AU at $t = 3 \times 10^6$ yr was at $R \gtrsim 200$ AU for the first 8×10^5 yr (Fig. 2). Because the collision timescale is $\tau_{\text{col(th)}} \gtrsim 8 \times 10^5$ yr for grains of radius 10^{-5} cm at $R \gtrsim 200$ AU, grains can hardly grow during this period even if the sticking probability is as high as unity. Thus, the molecular evolution is not much affected by the growth of grains at least at $t \lesssim 8 \times 10^5$ yr.

As the matter migrates further to the inner regions of higher density, the timescale of grain-grain collision decreases. Numerically, we have

$$\begin{aligned} \tau_{\text{col(th)}} &= 2.4 \times 10^6 \left(\frac{20 \text{ K}}{T}\right)^{1/2} \left(\frac{a}{10^{-4} \text{ cm}}\right)^{5/2} \\ &\quad \times \left(\frac{0.0102}{\xi}\right) \left(\frac{10^{10} \text{ cm}^{-3}}{n_{\text{H}}}\right) \text{ yr}, \end{aligned} \quad (13)$$

where $n_{\text{H}} = 10^{10} \text{ cm}^{-3}$ corresponds to the density at $R \sim 50$ AU in our disk model. Thus, at $t \sim 3 \times 10^6$ yr grains in the accreting matter can be as large as $a \sim 10^{-4}$ cm, and the formation of CO_2 ice, HCN ice, and H_2CO ice will be suppressed in this later stage. Thus, according to Figure 8b, the abundances of HCN ice and CO_2 ice at $t = 3 \times 10^6$ yr can be as low as $n(i)/n_{\text{H}} \sim 10^{-6}$ in the region of $R = 10$ – 90 AU. The abundances of CH_4 and NH_3 ices are scarcely affected by the grain growth as long as the grain radius $a \lesssim 10^{-4}$ cm.

When the turbulence ceases, the accretion flow would also stop because angular momentum transport is not expected in the disk. The growth of grains will be accelerated in such situation. Once the disk becomes quiet enough, grains begin to sediment toward the midplane of the disk. The sedimentation velocity of the grain is determined by the balance between the gas-drag force and the vertical component of the stellar gravity acting on the grain and is proportional to the grain radius. Thus, larger grains sink faster and collide with smaller grains, which are sinking more slowly. According to Nakagawa, Nakazawa, & Hayashi (1981) the collision time at height Z from the midplane is

given by

$$\tau_{\text{col(sed)}} \approx \frac{2}{3\pi\xi} \frac{H}{Z} t_K \approx 7.4 \times 10^3 \left(\frac{0.0102}{\xi} \right) \times \left(\frac{H}{Z} \right) \left(\frac{R}{50 \text{ AU}} \right)^{3/2} \left(\frac{M_*}{1 M_\odot} \right)^{-1/2} \text{ yr}, \quad (14)$$

where t_K is the Keplerian orbital period. The collision time-scale is independent of the grain size. Because $\tau_{\text{col(sed)}}$ is very small, the grains would grow very rapidly, and thus the molecular evolution would be much slower in the post accretion phase than in the accretion phase if the sticking probability in grain-grain collision is $\gtrsim 10^{-2}$. Precisely speaking, this effect of grain growth will be somewhat compensated for by the higher dust/gas ratio near the midplane due to the sedimentation of dust grains, and by the fluffiness of the dust aggregates, which causes a larger surface area than in the case of compact grains.

3.3.3. Initial Abundances of Molecules

So far we have assumed that initially carbon is in CO, nitrogen is in N_2 , and the remaining oxygen is in H_2O ice (called Model A). In this subsection we discuss the dependence of our results on the initial conditions by comparing with the results for another set of the initial molecular abundances, which we call Model B. Table 2 shows the initial molecular abundances in Model B; the initial molecular abundances in the gas phase were determined by referring to the observations of TMC-1 (Irvine, Goldsmith, & Hjalmarson 1987) and those in ice mantles by referring to the observations of luminous young stellar objects and field stars through molecular clouds by ground-based infrared telescopes and the Infrared Space Observatory (ISO) (Whittet 1993; Whittet et al. 1996; van Dishoeck 1998; Whittet et al. 1998). As for the elemental abundances we

TABLE 2

THE INITIAL MOLECULAR COMPOSITION FOR MODEL B^a

Species	Abundance	Species	Abundance
N.....	4.06(-6) ^b	O.....	4.25(-6)
Si.....	9.74(-7)	S.....	9.13(-6)
Fe.....	2.74(-7)	Na.....	2.25(-7)
Mg.....	1.09(-6)	H ₂	5.00(-1)
C.....	2.64(-8)	N ₂	8.15(-6)
CH.....	1.00(-8)	OH.....	1.50(-7)
CO.....	3.97(-5)	CN.....	1.50(-8)
CS.....	5.00(-9)	SO.....	2.70(-9)
HCN.....	1.00(-8)	C ₂ H.....	4.00(-8)
OCS.....	1.00(-9)	H ₂ CO.....	1.00(-8)
NH ₃	1.10(-8)	HC ₃ N.....	3.00(-9)
CH ₃ CN.....	5.00(-10)	CH ₃ OH.....	2.00(-9)
HCO ⁺	4.00(-9)	N ₂ H ⁺	2.50(-10)
HCS ⁺	3.00(-10)	CO ice.....	2.15(-5)
H ₂ O ice.....	8.60(-5)	CO ₂ ice.....	1.29(-5)
NH ₃ ice.....	4.30(-6)	CH ₄ ice.....	1.72(-6)
CH ₃ OH ice.....	2.58(-6)		

^a The abundances are by number relative to hydrogen nuclei.

^b $a(b)$ means $a \times 10^b$.

adopt the same values as in Model A, or in Table 1. All the elements that are not in molecular form are assumed to be in atomic form, except for hydrogen and nitrogen. Hydrogen is assumed to be in H_2 . Four-fifths of the remaining nitrogen is assumed to be in N_2 and one-fifth in atomic form referring to the theoretical models in molecular clouds (e.g., Millar, Farquhar, & Willacy 1997).

Figures 9 and 10 show the evolution of molecular abundances in the matter which migrates from 395 to 10 AU in 3×10^6 yr for Model B. Comparing these with Figures 2 and 4 for Model A we find that the molecular abundances in Model B are similar to those in Model A except for the

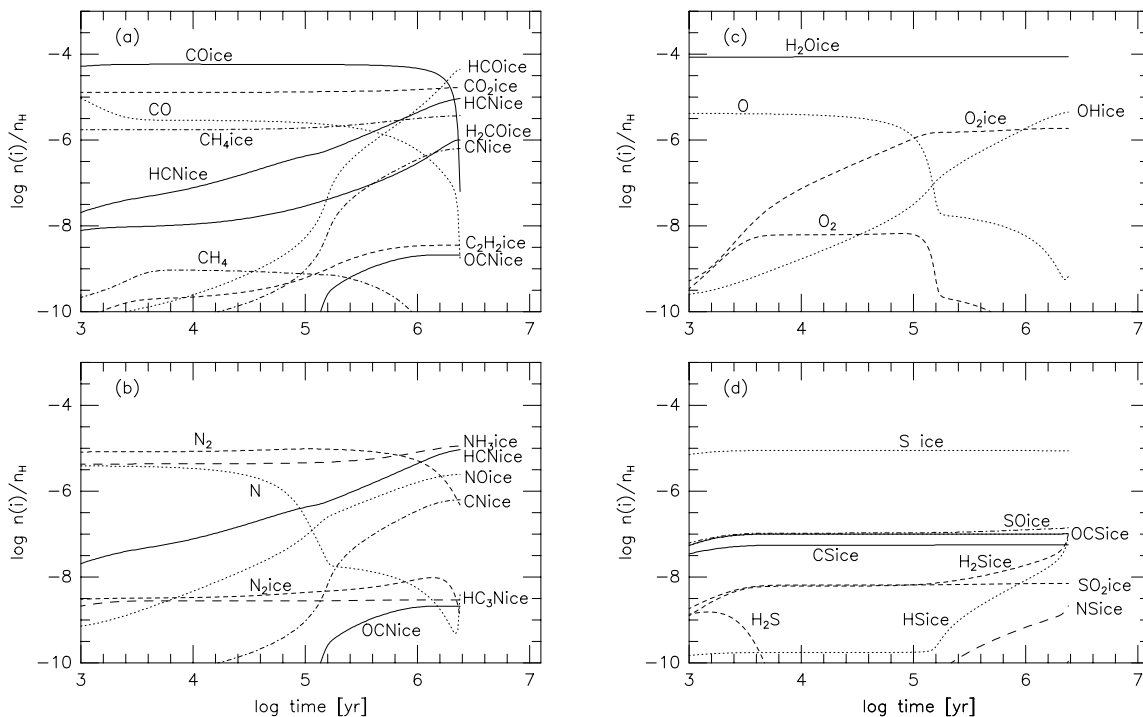


FIG. 9.—Evolution of molecular abundances in the matter which migrates from $R = 395$ AU to $R = 54$ AU in 2.4×10^6 yr for Model B (the initial molecular abundances determined referring to the observations of gaseous species in TMC-1 and the observations of interstellar ices; Table 3). The other details are the same as in Fig. 2.

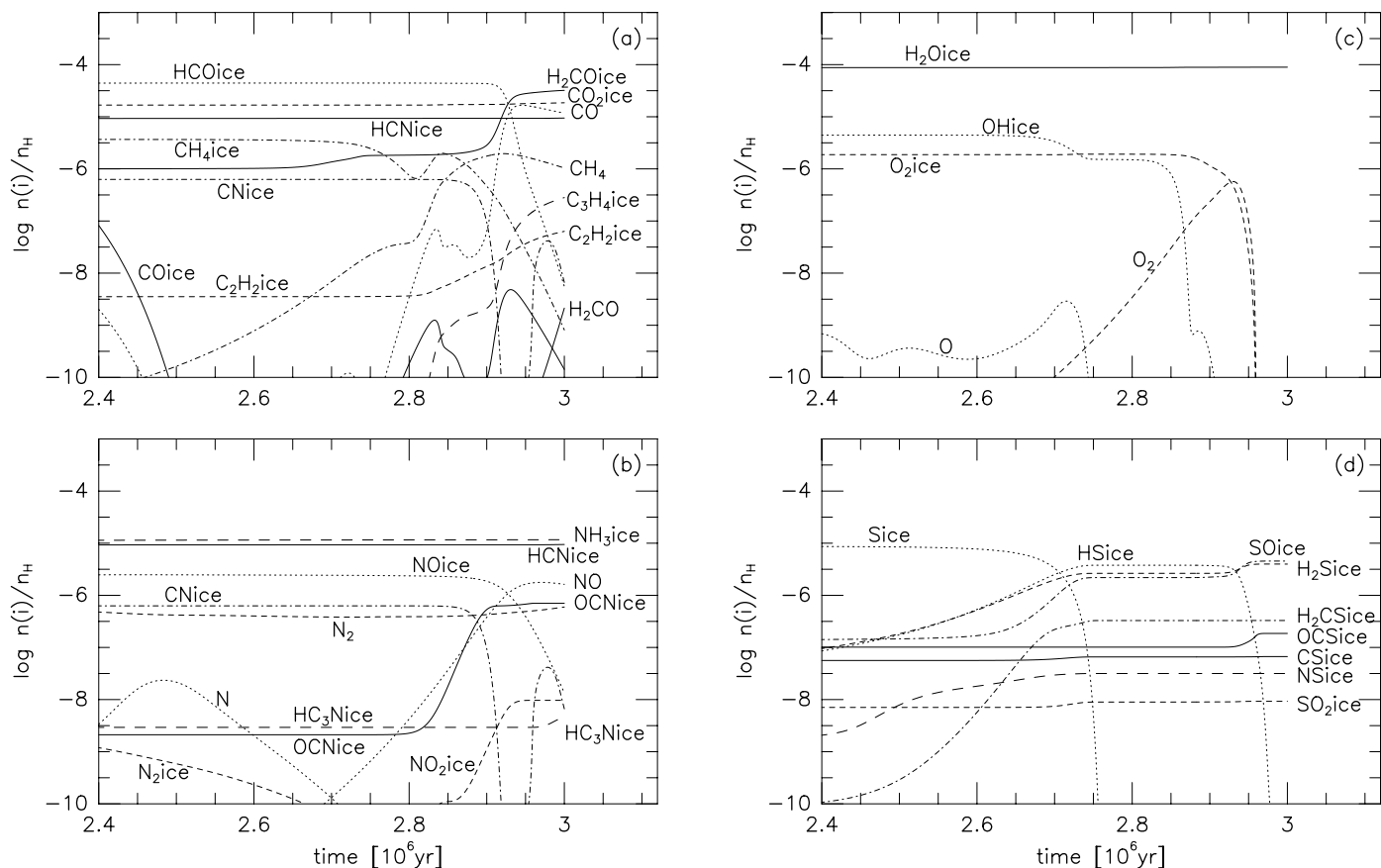


FIG. 10.—Evolution of molecular abundances in the matter which migrates from $R = 54$ AU to $R = 10$ AU for model B in the period between $t = 2.4 \times 10^6$ and 3×10^6 yr after the final stage of Fig. 9. The other details are the same as in Fig. 4.

following two points. First, in the early stages in Model B, HS ice is considerably less abundant, and SO_2 ice and NO_2 ice are more abundant. These differences are caused by O atoms, which are initially more abundant in Model B. By reaction with an O atom HS in the gas phase is transformed into SO, which reacts again with O to produce SO_2 . After O atoms are transformed into O_2 (at $t \gtrsim 2 \times 10^5$ yr), HS ice increases considerably. Since O_2 is also more abundant in Model B, NO_2 is formed more efficiently by the reaction of NO with HO_2 , whose precursor is O_2 .

The second point concerns the origin of ice mantles. In Model B, significant amounts of ices were assumed to exist initially in accordance with the observations, which we call the ices of interstellar origin. Most of the molecules in ice mantles do not react with other species in 3×10^6 yr. Comparing the final or peak abundances of some ices with their initial abundances we find that most of H_2O ice, two-thirds of CO_2 ice, half of CH_4 ice, and one-third of NH_3 ice are of interstellar origin. This suggests that a significant fraction of the ice mantles, especially H_2O ice, in the protoplanetary disks can be of interstellar origin. However, it should be noted that there still remain some uncertainties in the composition of the interstellar ice. No stringent limit on the amount of the interstellar NH_3 ice is given because its absorption band blends with other features. Interstellar CH_4 ice is difficult to observe from the ground because of telluric contamination. Since the ISO observations of ices were only toward luminous young stars, except for CO_2 ice, which was obtained toward Elias 16, it may be possible that its observational data trace not only interstellar ices in

quiescent clouds but also matter in warm circumstellar shells, which was processed in a similar way as described in our model.

Figure 11 shows the spatial distribution of molecular abundances in the disk at $t = 3 \times 10^6$ yr for Model B. Despite the differences in the initial abundances, the distribution at this stage is similar to that for Model A, except for the following minor differences. In the outer regions $R \gtrsim 50$ AU, CO, both in gas phase and in ice, is more heavily depleted in Model B than in Model A. This is because reactive species (e.g., O atom) with CO are initially more abundant in Model B. The boundary between the CO-rich and CO-depleted regions depends not only on the temperature, but also on the rate of CO destruction. Since the timescale of desorption is short near the boundary, the boundary is determined by the competition between CO destruction and migration. In Model B, OCS ice is less abundant because it is formed by the reaction of S with CO, which is less abundant than in Model A.

We have also performed calculation with another set of elemental abundances; the low-metal model in which the elemental abundances of S, Si, Mg, Fe, and Na are lower by 2 orders of magnitude (e.g., Lee et al. 1998). The initial molecular abundances are essentially the same as in Model B. We have found that the results are similar to those in Figures 9, 10, and 11 for C-, N-, and O-bearing molecules. While the absolute abundances of S-bearing molecules are 2 orders of magnitude lower in the low-metal model than in Model B, the relative abundances among S-bearing molecules are very similar to those in Model B except for CS

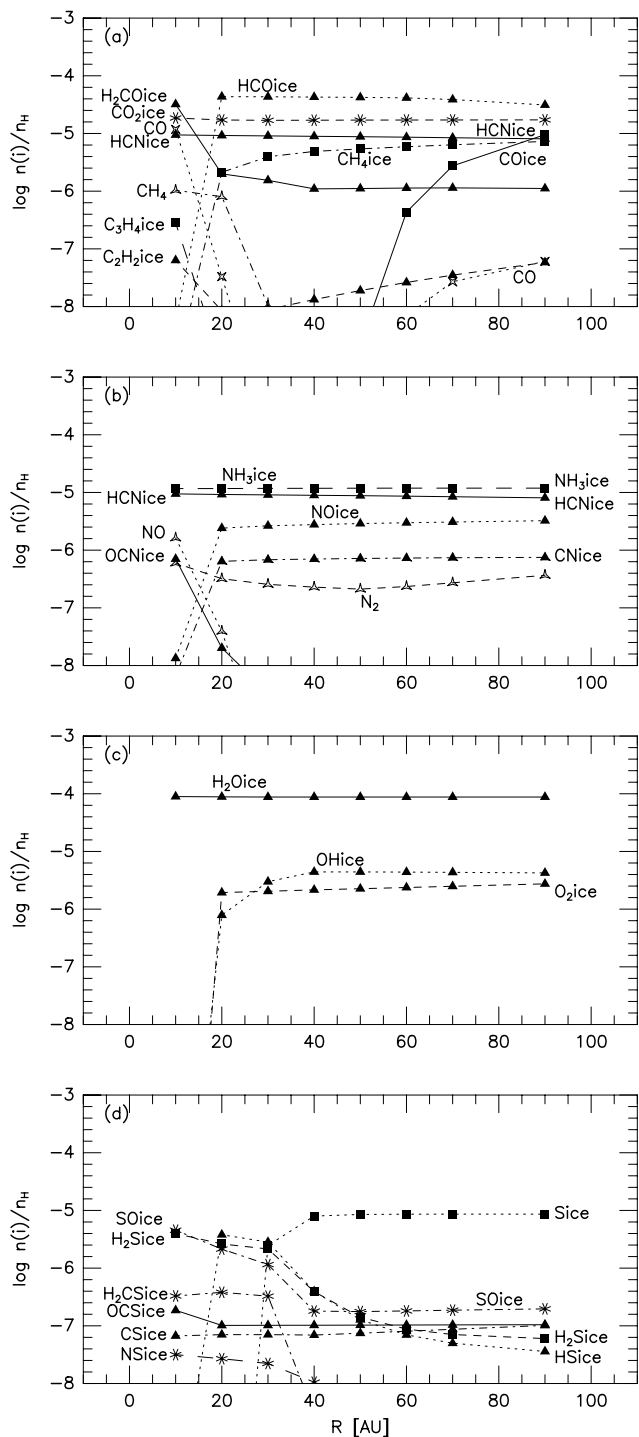


FIG. 11.—Distribution of molecular abundances in the accretion disk at $t = 3 \times 10^6$ yr for Model B. The other details are the same as in Fig. 5.

ice, which is relatively more abundant ($n(\text{CS ice})/n_{\text{H}} \sim 10^{-8}$) because of its high initial abundance.

From these results, we can conclude that the main results described in the previous subsections hardly depend on the initial molecular abundances.

4. DISCUSSION

4.1. Comparison with Previous Works

The molecular composition obtained in our model is quite different from that in the KI model. We have found that a considerable amount of CO, which originally came

from the interstellar cloud, is transformed into other C-bearing molecules. At the final stage $t = 3 \times 10^6$ yr of our model 10^{-2} – 10^{-1} of carbon is in CH_4 ice and CO_2 ice. On the other hand, in the original KI model only 10^{-7} of carbon is in CH_4 ice and less than 10^{-2} of carbon is in CO_2 ice. Similarly, about 0.3 of nitrogen is in NH_3 ice in our model, while only 10^{-5} of nitrogen is in NH_3 ice in the KI model. One of the reasons for these differences is in our taking into account the cosmic-ray ionization, which drives molecular evolution by producing ions and radicals. We have also taken into account the adsorption and desorption of molecules on grain surface in the time-dependent equations together with the chemical reactions. In contrast, in the KI model, molecular abundance is determined at the quenching radius ($R < 1$ AU) where the temperature is high (see § 1), and adsorption and desorption in the matter transported to the outer region is treated in an equilibrium manner. In our model, CO is transformed into CH_4 and CO_2 , and N_2 into NH_3 , which accumulate in the ice mantles, since they are less volatile than CO and N_2 . This is another reason for the higher ratios of $n(\text{CH}_4 \text{ ice})/n(\text{CO})$ and $n(\text{NH}_3 \text{ ice})/n(\text{N}_2)$ in our model than in the KI model.

Although the high abundance of hydrocarbons and NH_3 is also derived by W98, their model is different from ours. In W98, the temperature in the outer region of the disk ($R \gtrsim 40$ AU) is so low ($T \lesssim 10$ K), that the depletion onto grains is more severe than in our model. Instead of gas-phase reactions, grain-surface reactions play a dominant role at such low temperatures. It should be noted that the temperature in the outer region is underestimated by W98: they considered only the heating by mass accretion and neglected the heating by the central star, which is the dominant energy source at $R \gtrsim 10$ AU for $L_* \approx 1 L_{\odot}$ as shown in § 2.1. Thus, we think that the results of W98 for the outer region apply to disks around stars with lower luminosity ($L_* < 1 L_{\odot}$). The dependence of our result on the temperature distribution and the luminosity of the central star will be discussed in § 4.3.

4.2. Uncertainties in the Grain-Surface Recombination of HCO^+

One of the merits of solving directly the reaction equations is that we can distinguish the major reactions that determine the abundance of each molecule among thousands of reactions. Analyzing the reaction network, we have found that the key reaction which critically determines the transformation rate of CO to CO_2 , HCN, and H_2CO is the grain-surface recombination of HCO^+ . We have assumed that the grain-surface recombination occurs without dissociation as long as the resultant species are stable.

In this assumption HCO^+ is just neutralized to HCO, with the Coulomb energy of recombination deposited onto grain surface, while it is dissociated into CO and H by the gas-phase recombination. However, there are no direct evidences for or against this assumption at present. Therefore, we have also performed numerical calculation with another assumption that HCO^+ dissociates to H and CO as a result of the grain-surface recombination.

In Figure 12 we show the evolution of molecular abundances in the matter migrating from $R = 568$ to 70 AU in 3×10^6 yr in the two cases; HCO^+ recombines on grains (a) to form HCO and (b) to form CO and H atom. In the dissociative case (Fig. 12b) CO_2 ice and HCN ice are less abundant and CO is more abundant at $t = 3 \times 10^6$ yr com-

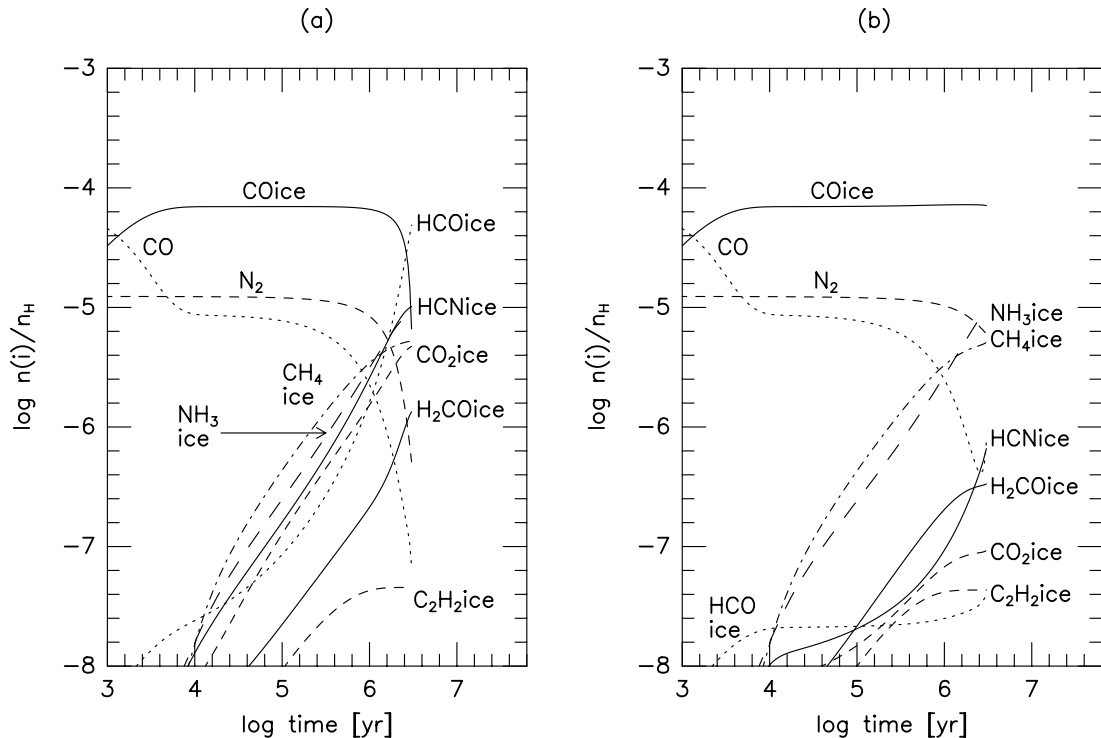


FIG. 12.—Evolution of molecular abundances in the matter which migrates from $R = 568$ to 70 AU in 3×10^6 yr. The product of the grain-surface recombination of HCO^+ is assumed to be (a) HCO (standard case) and (b) $\text{CO} + \text{H}$.

pared with Figure 12a. The abundances of CH_4 ice, hydrocarbon ice, NH_3 ice, and S-bearing molecules are not much affected, since they are formed through the other reactions. The S-bearing molecules are omitted in Figure 12 because they are similar to Figure 7b.

Figure 13 shows the distribution of molecules at $t = 3 \times 10^6$ yr for the dissociative case (b). Among C-bearing molecules, CO is the most abundant through $R = 10$ to 90 AU. The abundances of CO_2 ice, HCN ice, and H_2CO ice, whose precursors are HCO, are lower than those in Figure 13a (Fig. 5) by an order of magnitude. On the other hand, the distributions of the other species such as CH_4 ice, hydrocarbon ice, and NH_3 ice are similar to those in Figure 13a, since they are formed through the other reactions, which are irrelevant to HCO. Most sulphur is taken up by OCS ice in the inner regions because of the high CO abundance.

It should be emphasized that the grain-surface recombination is more important in the disks than in molecular clouds. The abundance ratio of negatively charged grains to free electrons is much larger in protoplanetary disks than in molecular clouds because of higher density (Umebayashi 1983). Therefore, collision of HCO^+ with charged grains is more important in protoplanetary disks than in molecular clouds. It should be investigated by laboratory experiments and/or computational chemical studies whether the grain-surface recombination is dissociative or not.

We have assumed in § 3 that HCO^+ recombines to form HCO. This assumption gives upper limits to the abundances of CO_2 , HCN, and H_2CO and a lower limit to the abundance of CO.

4.3. Dependence on the Disk Model

As a typical case we have adopted $L_* = 1 L_\odot$ as the luminosity of the central star, $\dot{M} = 10^{-8} M_\odot \text{ yr}^{-1}$ as the

mass accretion rate of the disk, and the coefficient of viscosity $\alpha = 0.01$. Here we briefly discuss the effects of these quantities on the molecular evolution.

Molecular evolution crucially depends on the temperature in the disk. Since the luminosity of the central star is a major factor in determining the temperature distribution, molecular abundance would be quite different in disks with different luminosity of the central star. The effect of the stellar luminosity can be estimated roughly by scaling the molecular distribution shown in, e.g., Figure 5 with the temperature rather than with the distance from the central star. For example, CH_4 ice is abundant in the regions of $T \lesssim 28$ K, and the larger hydrocarbon ices are abundant in the regions of $T \gtrsim 28$ K as seen in Figure 5 (see also § 5.1). This boundary for the distribution of the two kinds of molecules must also locate at an annulus of $T \approx 28$ K for the other values of L_* though the radius of this annulus depends on L_* .

The sublimation temperatures of the most volatile molecules such as CO (~ 20 K) and N_2 (~ 16 K) provide important criteria for the molecular evolution. If the temperature in the disk is so low that even the most volatile species such as CO and N_2 do not evaporate, the chemical reactions in the gas-phase are suppressed, and chemical reactions on the grain surface will dominate as investigated by W98. Such a condition would apply to disks around stars with lower luminosity ($L_* < 1 L_\odot$).

Besides the luminosity of the central star, the temperature distribution also depends on the dust opacity in the disk, which can be a source of uncertainty. Since temperature is such a critical parameter for the molecular evolution, it would be best if the temperature distribution were to be ultimately determined by observation. However, to date there are significant differences between the values of temperature derived from different observations. While Beck-

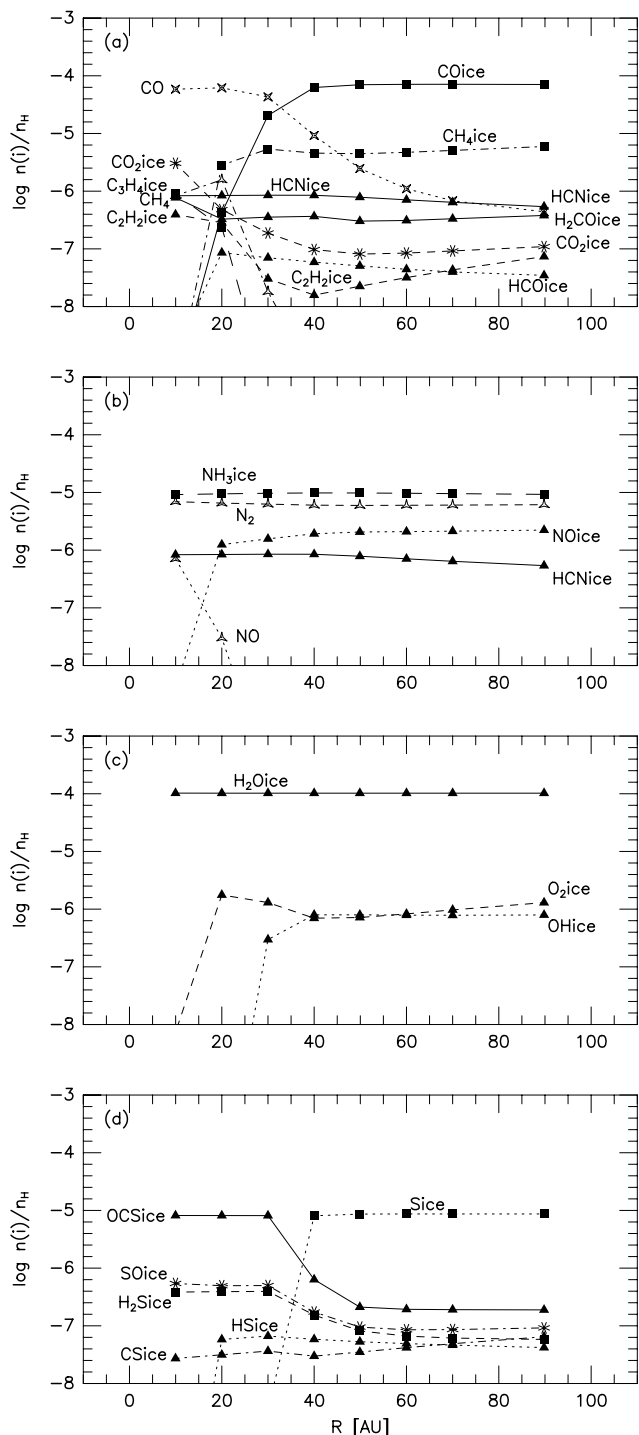


FIG. 13.—Distribution of molecular abundances in the accretion disk at $t = 3 \times 10^6$ yr. The product of the grain-surface recombination of HCO^+ is assumed to be $\text{CO} + \text{H}$. The other details are the same as in Fig. 5.

with et al. (1990) estimated the temperature at 100 AU, $T_{100\text{AU}}$, to be 10 K for DM Tau and 15 K for GM Aur from the spectral energy distribution of continuum emission, Guilloteau & Dutrey (1998) estimated $T_{100\text{AU}} = 32$ K for DM Tau, and Dutrey et al. (1998) estimated $T_{100\text{AU}} = 37$ K for GM Aur based on the aperture synthesized image of the CO emission line.

The competition between the accretion flow and the chemical reactions also determines the molecular abun-

dances in the disk. If the accretion rate is so high that most of the matter accretes onto the central star in a timescale much shorter than 10^6 yr, which is the typical chemical timescale for CO and N_2 , the molecular abundances are hardly affected by chemical reactions except for the highly active species such as atoms for which chemical timescales are much shorter. In such a situation the molecular abundances in the disk would be similar to that in molecular clouds and hardly vary with radius in contrast to those described in § 3 (see also § 5.2).

5. COMPARISON WITH OBSERVATIONS

5.1. Chemical Compositions of Comets

It is widely accepted that comets are one of the most pristine objects in the solar system, preserving a large amount of volatile material such as water. They are now considered to be the remnants of icy planetesimals formed in the outer region ($R \gtrsim 20$ AU) of the solar nebula. Here we compare the molecular abundances in our model disk with those in comets and discuss what comets tell us about the early stages of the solar system.

In this comparison we have to bear in mind that there are some uncertainties in determining the composition of comets. It is difficult to directly detect molecules in cometary nuclei. Instead, we observe molecules and radicals (daughter molecules) which are formed in the comae via photolysis induced by the solar UV radiation, and we estimate the molecular composition (parent molecules) in the cometary nuclei using chemical reaction models. Thus, the molecular composition derived from the observations is somewhat dependent on the model. In addition it is quite unclear whether the cometary nuclei are chemically homogeneous, and how much they were reprocessed in their formation stages and during their stay in the Oort cloud or in the Kuiper belt. There are several evidences indicating the presence of macroscopic internal heterogeneity in cometary nuclei. For example, in the observations of comet Halley, the relative production rate of H_2CO and H_2O varied more than tenfold, and outbursts were observed for some kinds of species, such as CO_2 -rich outbursts (Mumma, Weissman, & Stern 1993). Since further consideration of these uncertainties is out of the scope of this paper, we make a comparison assuming that the molecular abundances derived from the observations represent the bulk and pristine composition of cometary nuclei.

5.1.1. Origin of Cometary Ice

Table 3 shows the molecular abundances of the recent comets taken from Mumma et al. (1993), Feldman et al. (1996), Weaver et al. (1996), Lis et al. (1996), and Crovisier (1998). The abundances are expressed as the numbers of molecules on a scale for which water ice, the most abundant species in comets, is 100. Among C-bearing molecules, CO is the most abundant and CO_2 is also observed. Methane was observed in several comets, but it was not detected in comet Levy (Mumma et al. 1993 and references therein). Ammonia NH_3 was directly detected for the first time in comet Hyakutake with the abundance 0.0025 relative to water (Lis et al. 1996). Several kinds of S-bearing molecules were also detected in comet Hale-Bopp (Crovisier 1998 and references therein).

One of the most important characteristics of the molecular composition in comets is the coexistence of oxidized ice (e.g., CO and CO_2) and reduced ice (e.g., CH_4 and

TABLE 3
ABUNDANCES OF VOLATILE SPECIES IN THE RECENT COMETS

Species	Relative Abundance ^a	Object	Comments
H ₂ O.....	100		
CO	~7-8	Comet P/Halley	
	20	West (1976 VI)	
	2	Bradfield (1979 X)	
	1-3	Austin (1990 V)	
	20	Hale-Bopp	
H ₂ CO.....	0-5	Comet P/Halley	variable
	0.04	Levy (1990 XX)	if a parent molecule
	0.1	Autsin (1990 V)	if a parent molecule
	~1	Hale-Bopp	
CO ₂	3	Comet P/Halley	infrared obs. (Vega 1 IKS)
	6	Hale-Bopp	
CH ₄	<0.2-1.2	Comet P/Halley	ground-based infrared obs.
	0-2	Comet P/Halley	Giotto IMS; model dependent
	<0.2	Levy (1990 XX)	ground-based infrared obs.
	1.5-4.5	Wilson (1987 VII)	airborne infrared obs.
	0.7	Hyakutake	
	1	Hale-Bopp	
NH ₃	0.1-0.3	Comet P/Halley	variable; based on obs. of NH ₂
	1-2	Comet P/Halley	Giotto IMS
	0.25	Hyakutake	
	0.6	Hale-Bopp	
HCN.....	0.1	Comet P/Halley	variable; ground-based radio
	<0.02	Comet P/Halley	Giotto IMS
	0.2	Hale-Bopp	
	0.03-0.2	several comets	
N ₂	~0.02	Comet P/Halley	ground-based N ₂ ⁺ emission
H ₂ S	1.6	Hale-Bopp	
SO	0.6	Hale-Bopp	
SO ₂	0.15	Hale-Bopp	
OCS	0.5	Hale-Bopp	

^a The abundance is by number on a scale for which H₂O, which is observed in all the comets, is 100.

hydrocarbon), as pointed out by Yamamoto (1991) and as can be seen in Table 3. As shown in the previous sections, this coexistence in the protoplanetary disk is naturally realized by taking into account the cosmic-ray ionization in the disk. Via ion-molecule reactions, both CO₂ and CH₄ are produced from CO, which originally came from the molecular cloud. The abundances of CH₄, NH₃, and CO₂ relative to H₂O are \gtrsim a few $\times 10^{-2}$ at $t \gtrsim 10^6$ yr, which are consistent with the observed compositions of the comets (Table 3). Carbon monoxide and N₂ would also coexist in ice mantles even in the region of $R \lesssim 40$ AU because they can be physically *trapped* in water ice (Bar-Nun et al. 1985), although this effect was omitted in our calculation.

Some other models have been proposed as regards the origin of cometary ice. The original KI model cannot explain the coexistence of oxidized ice and reduced ice; in this model CH₄/CO $\sim 10^{-7}$ and NH₃/N₂ $\sim 10^{-5}$ (Prinn 1993 and references therein). Prinn & Fegley (1989) proposed that these reduced molecules were formed by the Fischer-Tropsch-type reactions, which are the catalytic reactions on the clean surface of metallic Fe and can produce hydrocarbons from CO and H₂. They also proposed that reduced molecules in the comets were produced in the circumplanetary nebula, where the pressure might have been much higher than in the protoplanetary disk. Applying the KI model to the circumplanetary nebula, Prinn & Fegley (1989, and references therein) obtained the

abundance ratios of reduced ice to oxidized ice CH₄/CO $\sim 10^6$ and NH₃/N₂ ~ 1 . However, to take this matter into comets, some mechanism is required to mix the matter processed in the circumplanetary nebulae with the material in the protoplanetary disk.

The interstellar ice residue model has been proposed to explain the origin of cometary ice (Greenberg 1982; Yamamoto et al. 1983; Yamamoto 1985; Mumma et al. 1993). In this model, the formation of cometary ice is divided roughly into two stages. The first is the interstellar-cloud stage, in which gaseous molecules in the cloud condense onto grain surfaces. The second is the solar-nebula stage, in which very volatile species such as CO and N₂ are lost by sublimation from the ice mantles since the solar nebula is warmer than the interstellar cloud. While our model is similar to the interstellar ice residue model in that the interstellar ice contributes to the abundances of the molecules in comets which are scarcely desorbed (§ 3.3), the difference is that in our model chemical reactions are taken into account in the disk in addition to sublimation of ice mantles. Our model predicts that a significant amount of molecules is produced in the disk in addition to the interstellar components. Observations of carbon-chain molecules in comets suggest that chemical reactions occurred in the solar nebula, as will be mentioned in the next subsection.

In summary, our model reproduce some comet observations more naturally than the previous models. Our

model also shows that the grain size and the cosmic-ray flux critically determine the production rates of molecules in the protoplanetary disks. If we could know how much molecules were produced in the solar nebula by comparing cometary ice with interstellar ice in detail, we might be able to give constraints on the cosmic-ray flux, the ionization state, and the timescale of grain growth in the solar nebula.

5.1.2. Chemical Variation and Formation Site of Comets

An array of observational evidence is accumulating in support of the idea that comets exhibit internuclear heterogeneity. The ratios of the production rates among various molecules vary strongly from comet to comet (Table 3). Although the variability may be related to processing at comet surfaces and insolation after the formation, the most important cause must be in cosmogonic differences, or the molecular composition of each comet must depend strongly on where it was formed. Indeed, our results show that the molecular composition in the disk varies with the distance from the central star. We now discuss the possibility of estimating the formation site of each comet from its molecular composition.

First of all, we can make use of the fact that the abundances of some molecules in ice mantles change drastically around the annulus where the temperature is equal to its sublimation temperature (sublimation front). Figure 14 shows the sublimation fronts of some kinds of species. Since the temperature distribution in the disk depends on the luminosity of the central star, the positions of the fronts are shown as functions of the stellar luminosity. In the case of $L_* = 1 L_\odot$, for example, CH_4 would be abundant in the comets formed at $R \gtrsim 20$ AU, but would be depleted in the comets formed at $R \lesssim 20$ AU (see also Fig. 5). The abundance of CO shows a similar behavior; its abundance is almost constant in the outer regions and begins to decrease at $R \sim 40$ AU, where the temperature is equal to its sublimation temperature (~ 20 K).

Second, our model shows that some kinds of species, such as C_3H_4 ice, are *more* abundant in the *inner* regions. Since they are formed from the precursors such as CO and CH_4 , their abundances increase as R decreases inside the sublimation fronts of the precursors, take the peak values

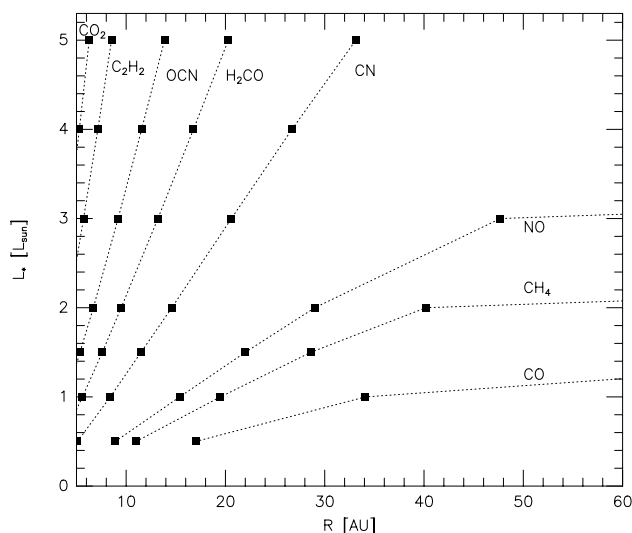


FIG. 14.—Sublimation fronts of some molecules as functions of the stellar luminosity.

around their sublimation fronts, and then decrease as R decreases. Thus, comets with more C_3H_4 must have formed in the inner regions than those with less C_3H_4 . Similarly, CO_2 and H_2CO are more abundant inside the sublimation front of HCO (at $R \sim 20$ AU) than outside.

It is to be noted that the spatial distribution of the molecules such as C_3H_4 mentioned above cannot be obtained in the models without chemical reactions in the disk. If all the volatiles in comets were unprocessed interstellar matter as in the interstellar ice residue model, the molecular composition in comets would depend on the formation site only through sublimation, not through chemical reactions of the sublimated species; for example, the comets with more C_3H_4 would have been formed in the outer regions than those with less C_3H_4 , conversely to our model.

Observing 85 comets over a period of 17 years and investigating the molecular production rates in each comet, A'Hearn et al. (1995) found that the group of comets called "Jupiter's family" is depleted in carbon-chain molecules, such as C_2 and C_3 , by a factor of 20 compared with the other groups. They argue that most of the Jupiter-family comets came originally from the Kuiper belt outside the Neptune and Pluto orbits, while most of the non-Jupiter-family comets, such as the Halley-family and long-period comets, came originally from the region of Uranus and Neptune, on the basis of the statistical study on the orbital evolution. Their result suggests that carbon-chain molecules or their parent molecules were *more abundant* in the *inner* region of the solar nebula. Since the large hydrocarbons, C_2H_2 and C_3H_4 , can be the parent molecules of these carbon-chain molecules, their conclusion is consistent with our model with chemical reactions in the protoplanetary disk and is not consistent with the interstellar residue ice model.

5.2. Future Observations of Protoplanetary Disks with Molecular Lines

One of the most important progresses in the recent radio astronomy is the development of the observational techniques at submillimeter wavelengths. For example, the submillimeter array (SMA) is now under construction on Mauna Kea.

One of the advantages of the observations at higher frequencies is higher spatial resolution. With the expected sensitivity of the telescope, an angular resolution of about $1''$ will be available at SMA, while it is about a few arcseconds with the existing interferometers at mm wavelengths. An angular resolution of $1''$ corresponds to a spatial resolution of about 140 AU for the nearest star-forming region (Taurus molecular cloud) at 140 pc from the earth. As for the spatial resolution, we can expect further progress in the near future. The Large Millimeter and Submillimeter Array (LMSA) and the Millimeter Array (MMA) have recently been proposed. These projects aim at an angular resolution of about $0''.05$, which corresponds to a spatial resolution of 7 AU for the Taurus molecular cloud. On the basis of our results we here give some expectations for the future observations with such high spatial resolution.

It should be born in mind, however, that in this paper we have investigated the molecular abundances only near the midplane of the disk. The surface layers may have quite different molecular abundances because the density is much lower than at the midplane and the matter is irradiated with UV radiation and X-rays. Although the mass contained in

the surface layers is significantly smaller than the total mass of the disk, they may considerably affect the intensities and profiles of the molecular emission lines from the disk (Aikawa et al. 1996). We have to fully calculate the vertical distribution of molecules in the disk for more direct comparison with observations. The vertical distribution of CO molecules in the outer region $R \gtrsim 100$ AU of the disk and comparison with observational data is described in Aikawa et al. (1996). The vertical distribution of other molecules will be reported in the forthcoming paper.

5.2.1. Dissipation of Gaseous Component

By the observations of molecular lines from many protoplanetary disks we might be able to find out statistically when and how the gaseous component in the disks disappears. Since Jovian planets should have formed in the gaseous disk, knowledge on the dissipation of the gaseous component will give us a critical constraint on the formation timescale of the Jovian planets in the planetary systems (§ 1).

In this and our previous papers we have obtained the abundance of CO in the disk, which is the most frequently used probe in the radio observations of protoplanetary disks. We have found the abundance ratio in the gas phase $n(\text{CO})/n_{\text{H}} \sim 10^{-4}$ in the region of $T \gtrsim 20$ K ($R \lesssim 40$ AU) at $t \lesssim 10^6$ yr. For this region we can derive the amount of the gaseous component from the observations of the CO emission lines by adopting the constant conversion factor $n_{\text{H}}/n(\text{CO}) \sim 10^4$.

In the disk of age $t \gtrsim 10^6$ yr, CO might have been transformed into CO_2 and depleted in the region of $20 \text{ K} \lesssim T \lesssim 70 \text{ K}$ ($40 \text{ AU} \gtrsim R \gtrsim \text{several AU}$). Further investigation is needed to predict the abundance of CO in this region, such as an investigation of the branching ratio of grain-surface recombination of HCO^+ and observational study on the ionization state of the disk (see § 3.3 and § 4.2). In the region of $T \gtrsim 70$ K ($R \lesssim \text{several AU}$), CO can be abundant in the gas phase and coexist with CO_2 (Paper I) even at the age $t \gtrsim 10^6$ yr, because CO is formed anew from CO_2 , which sublimates around 70 K.

It should be noted again that we have investigated the abundance of CO only at the midplane. In the surface region of the disk, where the density is much lower, gaseous CO can be abundant even if the temperature is lower than the values stated above ($T \lesssim 20$ K for $t \lesssim 10^6$ yr and $T \lesssim 70$ K for $t \gtrsim 10^6$ yr). It means that gaseous CO may be detected even in the regions of low temperature, but we cannot estimate the amount of gaseous component from the intensity of CO emission lines in these regions because CO is significantly depleted near the midplane (Aikawa et al. 1996).

5.2.2. Temperature Distribution in the Disk

In addition to CO some other molecules, such as CN and CS, are observed in the protoplanetary disks (Dutrey et al. 1997). Since these molecules are less volatile and more easily accreted onto grains than CO, it seems difficult to estimate the total amount of gaseous component in the disk from the observation of their emission lines. However, our model shows that they can be a good indicator of the temperature. The abundance of a gaseous molecule sharply changes around its sublimation front, the position of which differs from molecule to molecule. Table 4 shows the sublimation temperatures of some molecules which are observable with radio telescopes. Thus, observations of various molecular

TABLE 4
SUBLIMATION TEMPERATURES
OF MOLECULES

Species	Sublimation Temperature (K)
CO	23
CN	38
CS	55
NH_3	85

lines with high spatial resolution will reveal the precise temperature distribution in the disk.

5.2.3. Accretion Velocity

The distribution of molecules in the disk depends on the accretion velocity. For example, CO is abundant even in the region of $20 \text{ K} \lesssim T \lesssim 70 \text{ K}$, if the timescale of accretion is smaller than the chemical timescale for CO-destruction, $t \sim 10^6$ yr (see also § 3.3). The molecules in the ice mantle evaporate when the matter migrates inside their sublimation front. The evaporated molecules exist and will be observed in an annular region whose width is approximately given by the product of the accretion velocity and the timescale for molecular destruction by chemical reactions. As an example we show in Figure 15 the distribution of H_2CO gas in the disk with $L_* = 5 L_{\odot}$ at $t = 3 \times 10^6$ yr, together with the distribution of the density and temperature. The accretion velocity $v_R \sim 10^{-4}$ AU yr $^{-1}$ is similar to that in the standard case ($L_* = 1 L_{\odot}$). The width

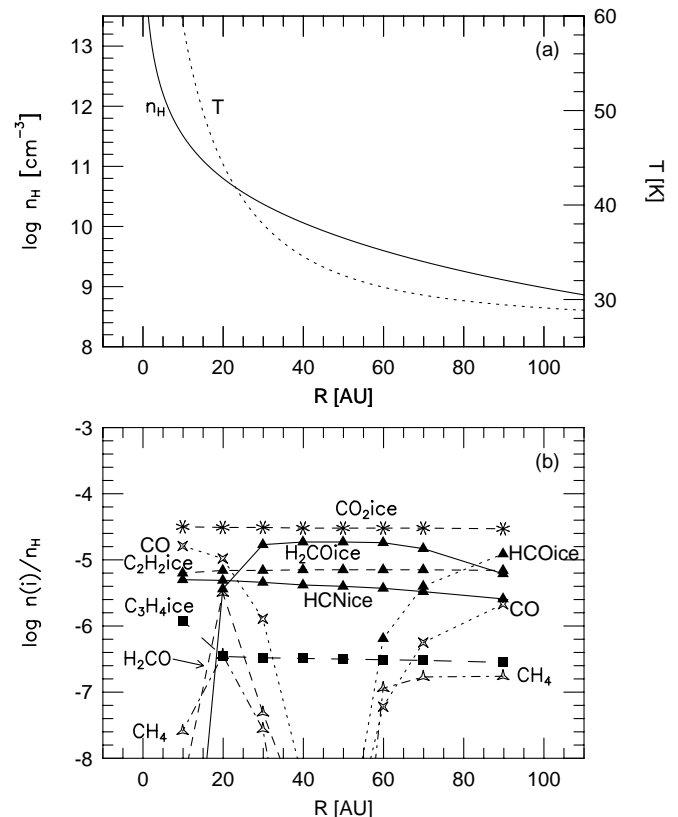


FIG. 15.—Distribution of molecular abundances in the accretion disk at $t = 3 \times 10^6$ yr for $L_* = 5 L_{\odot}$ (b). The other parameters are the same as in the standard case. Panel (a) shows the distribution of the density and the temperature in the disk.

of the region where H_2CO gas is abundant is ~ 10 AU because the abundance of H_2CO decreases in $\sim 10^5$ yr after desorption. Thus, we will be able to estimate the accretion velocity by observing the distribution of some molecules in the disk.

6. SUMMARY

We have investigated the evolution of the molecular composition in a protoplanetary disk in which matter is accreting toward the central star by solving numerically the reaction equations of molecules as an initial-value problem. We have obtained the molecular composition both in the gas phase and in ice mantles of grains as a function of time and position in the disk. The main results are as follows.

In the region of radius $R \gtrsim$ several AU, where the column density of the disk is smaller than the attenuation length of cosmic-ray ionization, $\sim 96 \text{ g cm}^{-2}$, the ions formed by cosmic-ray ionization play an important role in molecular evolution. A considerable fraction of CO, which came originally from the interstellar cloud, is destroyed by ion-molecule reactions and is finally transformed into CO_2 , HCN, H_2CO , and CH_4 . Similarly, N_2 is transformed into HCN and NH_3 . Formation of ice mantles is also important in molecular evolution. In the regions where the temperature is low enough for the products to freeze onto grains, they are adsorbed onto grains in a short timescale because of the high density in the disk and thus accumulate in ice mantles. Although molecular evolution proceeds in the protoplanetary disk, our model also shows that some amount of interstellar ice survives and contributes considerably to the molecular abundances in ice mantles in the disk. Especially, most of water ice in the disk is interstellar origin.

We have also found that the timescale for molecular evolution depends on the ionization rate and the grain size. If the ionization rate and the grain size are the same as those in the molecular clouds, the timescale in which CO and N_2 are transformed into the other species is estimated to be $\sim 10^6$ yr, which is slightly shorter than the lifetime of the disk. Since the molecular evolution is enhanced by ionization, the chemical timescale is larger in the case of lower ionization rate. Grains play critical roles in molecular evolution; by sticking to grains some products can survive, which would otherwise be destroyed by gas-phase reactions. Since the number ratio of negatively charged grains to free electrons is much higher in the protoplanetary disks than in the interstellar clouds, grain-surface recombination is more important in the disk. Grain-surface recombinations produce some molecules which are not formed by dissociative recombination in the gas phase. Since the colli-

sion rate with grains is inversely proportional to the grain radius, the production rates of some kinds of species depend on the grain size.

The spatial distribution of molecules depends crucially on the temperature distribution. For example, CH_4 ice is abundant in the region of $R \gtrsim 20$ AU, where the temperature is lower than its sublimation temperature ~ 28 K. In the inner region CH_4 is desorbed and the ice of larger hydrocarbon, which is formed from CH_4 , are abundant.

We have compared the molecular composition in ice mantles derived from our model with that in comets and have found that our model reproduces naturally the coexistence of oxidized ice and reduced ice, which is observed in comets. It is suggested that the formation site of each comet can be estimated from its molecular composition. For example, comets with abundant CH_4 must have formed at $R \gtrsim 20$ AU, while the comets with abundant carbon-chain molecules formed in the inner region. Detailed observations of molecular composition in comets will give a constraint on the cosmic-ray flux or the timescale of the grain growth in the early stages of our solar system, because the molecular abundances in the disk depend on the ionization rate and grain size.

We have expressed some expectations for the observations based on our results. The total amount of the gaseous component in the disk can be estimated from the observation of the CO emission lines by adopting the relative abundance of $n(\text{CO})/n_{\text{H}} \sim 10^{-4}$ obtained by our model at least in the region of $R \lesssim 40$ AU ($T \gtrsim 20$ K) for the disks of age $t \lesssim 10^6$ yr. Observations of various molecules such as CO, NH_3 , etc., with high spatial resolution can reveal the temperature distribution and the accretion velocity in the disk.

The authors are grateful to Profs. Y. Abe, T. Yamamoto, J. Watanabe, and E. Herbst for their critical comments and suggestions. The anonymous referee's comments were useful in improving the manuscript. Y. A. would like to acknowledge Prof. Y. Nakagawa for helpful discussions and continuous encouragement. She is also grateful for financial support of the Japan Society for Promotion of Science. This work was supported by a Grant-in-Aid for Scientific Research of the Ministry of Education, Science, Sports, and Culture, Japan (10640224). The Astrochemistry Program at The Ohio State University is supported by The National Science Foundation. Numerical calculations were carried out on the VPP300/16R and VX/4R at the Astronomical Data Analysis Center of the National Astronomical Observatory of Japan.

REFERENCES

- A'Hearn, M. F., Millis, R. L., Schleicher, D. G., Osip, D. J., & Birch, P. V. 1995, *Icarus*, 118, 223
 Aikawa, Y., Miyama, S. M., Nakano, T., & Umebayashi, T. 1996, *ApJ*, 467, 684
 Aikawa, Y., Umebayashi, T., Nakano, T., & Miyama, S. M. 1997, *ApJ*, 486, L51 (Paper I)
 Anders, E., & Grevesse, N. 1989, *Geochim. Cosmochim. Acta*, 53, 197
 Balbus, S. A., & Hawley, J. F. 1991, *ApJ*, 376, 214
 Bar-Nun, A., Hertman, G., Laufer, D., & Rappaport, M. L. 1985, *Icarus*, 63, 317
 Basri, G., & Bertout, C. 1993, in *Protostars and Planets III*, ed. E. H. Levy & J. I. Lunine (Tucson: Univ. Arizona Press), 543
 Beckwith, S. V. W., Sargent, A. I., Chini, R. S., & Güsten, R. 1990, *AJ*, 99, 924
 Bergin, E. A., & Langer, W. D. 1997, *ApJ*, 486, 316
 Brasseur, G., & Solomon, S. 1986, *Aeronomy of the Middle Atmosphere*, (Dordrecht: Reidel)
 Chokshi, A., Tielens, A. G. G. M., & Hollenbach, D. 1993, *ApJ*, 407, 806
 Clayton, D. D. 1985, *Nature*, 315, 633
 Crovisier, J. 1998, *Faraday Discussion*, 109, 437
 Diehl, R., et al. 1993, *A&AS*, 97, 181
 Dolginov, A. Z., & Stepinski, T. F. 1994, *ApJ*, 427, 377
 Dutrey, A., Guilloteau, S., & Guélin, M. 1997, *A&A*, 317, L55
 Dutrey, A., Guilloteau, S., Prato, L., Simon, M., Duvert, G., Schuster, K., & Ménard, F. 1998, *A&A*, 338, 63
 Dutrey, A., Guilloteau, S., & Simon, M. 1994, *A&A*, 286, 149
 Farquhar, P. R. A., & Millar, T. J. 1993, *CCP7 Newsl.*, 18, 6
 Feldman, P. D., Festou, M., Rodriguez, P. M., Gonzalez, R., Spratt, C. E., Paradowski, M. L., & Kronk, G. W. 1996, *IAU Circ.* 6370
 Finocchi, F., & Gail, H.-P. 1997, *A&A*, 327, 825
 Frank, J., King, A., & Raine, D. 1992, *Accretion Power in Astrophysics*, (Cambridge: Cambridge Univ. Press)
 Greenberg, J. M. 1982, in *Comets*, ed. L. L. Wilkening (Tucson: Univ. Arizona Press), 131

- Guilloteau, S., & Dutrey, A. 1994, *A&A*, 291, L23
———. 1998, *A&A*, 339, 467
Handa, T., et al. 1995, *ApJ*, 449, 894
Hartigan, P., Kenyon, S. J., Hartmann, L., Strom, S. E., Edwards, S., Welty, A. D., & Stauffer, J. 1991, *ApJ*, 382, 617
Hasegawa, T. I., & Herbst, E. 1993, *MNRAS*, 261, 83
Hawley, J. F., & Balbus, S. A. 1991, *ApJ*, 376, 223
Hayakawa, S., Nishimura, S., & Takayanagi, K. 1961, *PASJ*, 13, 184
Irvine, W. M., Goldsmith, P. F., & Hjalmarsen, A. 1987, in *Interstellar Processes*, ed. D. J. Hollenbach & H. A. Thronson, Jr. (Dordrecht: Reidel), 561
Kawabe, R., Ishiguro, M., Omodaka, T., Kitamura, Y., & Miyama, S. M. 1993, *ApJ*, 404, L63
Koerner, D. W., & Sargent, A. I. 1995, *AJ*, 109, 2138
Koerner, D. W., Sargent, A. I., & Beckwith, S. V. W. 1993, *Icarus*, 106, 2
Krügel, E., & Siebenmorgen, R. 1994, *A&A*, 288, 929
Kusaka, T., Nakano, T., & Hayashi, C. 1970, *Prog. Theor. Phys.*, 44, 1580
Lee, H.-H., Roueff, E., Pineau des Forets, G., Shalabiea, O. M., Terzieva, R., & Herbst, E. 1998, *A&A*, 334, 1047
Lepp, S. 1992, in *The Astrochemistry of Cosmic Phenomena*, ed. P. D. Singh (Dordrecht: Kluwer), 471
Lewis, J. S. 1974, *Science*, 186, 440
Lewis, J. S., Barshay, S. S., & Noyes, B. 1979, *Icarus*, 37, 190
Lewis, J. S., & Prinn, R. G. 1980, *ApJ*, 238, 357
Lis, D., et al. 1996, *IAU Circ.*, 6362
Lynden-Bell, D., & Pringle, J. E. 1974, *MNRAS*, 168, 603
Mahoney, W. A., Ling, J. C., Wheaton, W. A., & Jacobson, A. S. 1984, *ApJ*, 286, 578
Mathis, J. S., Rumpl, W., & Nordsieck, K. H. 1977, *ApJ*, 217, 425
Millar, T. J., Farquhar, P. R. A., & Willacy, K. 1997, *A&ASS*, 121, 139
Millar, T. J., Rawlings, J. M. C., Bennett, A., Brown, P. D., & Charnley, S. B. 1991, *A&ASS*, 87, 585
Morton, D. C. 1974, *ApJ*, 193, L35
Mumma, M. J., Weissman, P. R., & Stern, S. A. 1993, in *Protostars and Planets III*, ed. E. H. Levy & J. I. Lunine (Tucson: Univ. Arizona Press), 1177
Nakagawa, Y., Nakazawa, K., & Hayashi, C. 1981, *Icarus*, 45, 517
Prinn, R. G. 1993, in *Protostars and Planets III*, ed. E. H. Levy & J. I. Lunine (Tucson: Univ. Arizona Press), 1005
Prinn, R. G., & Fegley, B., Jr. 1989, in *Origin and Evolution of Planetary and Satellite Atmospheres*, ed. S. K. Atreya, J. B. Pollack, & M. S. Matthews (Tucson: Univ. Arizona Press), 78
Ruden, S. P., & Pollack, J. B. 1991, *ApJ*, 375, 740
Saito, M., Kawabe, R., Ishiguro, M., Miyama, S. M., Hayashi, M., Handa, T., Kitamura, Y., & Omodaka, T. 1995, *ApJ*, 453, 384
Sandford, S. A., & Allamandola, L. J. 1993, *ApJ*, 417, 815
Shakura, N. I., & Sunyaev, R. A. 1973, *A&A*, 24, 37
Share, G. H., Kinzer, R. L., Kurfess, J. D., Forrest, D. J., Chupp, E. L., & Rieger, E. 1985, *ApJ*, 292, L61
Shu, F. H., Johnstone, D., & Hollenbach, D. 1993, *Icarus*, 106, 92
Skrutskie, M. F., et al. 1993, *ApJ*, 409, 422
Spitzer, L., Jr., & Tomasko, M. G. 1968, *ApJ*, 152, 971
Stevenson, D. J. 1990, *ApJ*, 348, 730
Strom, K. M., Strom, S. E., Edwards, S., Cabrit, S., & Skrutskie, M. F. 1989, *AJ*, 97, 1451
Takeuchi, T., Miyama, S. M., & Lin, D. C. N. 1996, *ApJ*, 111, 42
Umebayashi, T. 1983, *Prog. Theor. Phys.*, 69, 480
Umebayashi, T., & Nakano, T. 1981, *PASJ*, 33, 617
van Dishoeck, E. F. 1998, *Faraday Discussion*, 109, 31
Weaver, H. A., et al. 1996, *IAU Circular*, 6374
Weidenschilling, S. J., & Cuzzi, J. N. 1993, in *Protostars and Planets III*, ed. Levy, E. H., & Lunine, J. I. (Tucson: Univ. Arizona Press), 1031
Whittet, D. C. B. 1993, in *Dust and Chemistry in Astronomy*, ed. T. J. Millar & D. A. Williams (London: Inst. Phys. Publ.), 9
Whittet, D. C. B., et al. 1996, *A&A*, 315, L357
Whittet, D. C. B., et al. 1998, *ApJ*, 498, L159
Willacy, K., Klahr, H. H., Millar, T. J., & Henning, Th. 1998, *A&A*, 338, 995 (W98)
Yamamoto, T. 1985, *A&A*, 142, 31
———. 1991, in *Comets in the Post-Halley Era*, ed. R. L. Newburn, Jr., et al. (Dordrecht: Kluwer), 361
Yamamoto, T., Nakagawa, N., & Fukui, Y. 1983, *A&A*, 122, 171